ERT NASA CR-152473

Document P-1282 F
Final Report
Contract No. NAS5-20746
September 1976

Prepared for
Goddard Space Flight Center
Greenbelt, Maryland 20771

High resolution radiometric measurements of convective storms during the GATE experiment

Prepared by
Mary Grace Fowler
Anthony S. Lisa

ENVIRONMENTAL RESEARCH & TECHNOLOGY, INC.
CONCORD, MASS • CHICAGO • LOS ANGELES • WASHINGTON, D.C.

1. Report No.	2. Government Accession No.	3. Recipient's Catalog No.

4. Title and Subtitle	5. Report Date
High resolution radiometric measurements of convective storms during the GATE experiment	September 1976
	6. Performing Organization Code
7. Author(s)	8. Performing Organization Report No.
Mary Grace Fowler and Anthony S. Lisa	P-1282
	10. Work Unit No.
9. Performing Organization Name and Address	
Environmental Research & Technology, Inc. 696 Virginia Road Concord, Massachusetts 01742	11. Contract or Grant No. NAS5-20746
	13. Type of Report and Period Covered
12. Sponsoring Agency Name and Address	
National Aeronautics & Space Administration Washington, D.C. 20546	14. Sponsoring Agency Code

15. Supplementary Notes

Technical Officer: Dr. Thomas T. Wilheit, Jr.
Goddard Space Flight Center
Greenbelt, Maryland 20771

16. Abstract

Using passive microwave data from the NASA CV-990 aircraft and radar data collected during the Global Atmospheric Research Program Atlantic Tropical Experiment (GATE), an empirical model was developed relating brightness temperatures sensed at 19.35 GHz to surface rainfall rates. This model agreed well with theoretical computations of the relationship between microwave radiation and precipitation in the tropics. Analysis also showed that this relationship could be used with satellite microwave data to infer spatially averaged rain rates. The GATE aircraft microwave data was then used to determine the detailed structure of convective systems. The high spatial resolution of the data permitted identification of individual cells which retained unique identities throughout their lifetimes in larger cloud masses and allowed analysis of the effects of cloud merger.

17. Key Words (Suggested by Author(s))	18. Distribution Statement
Precipitation GARP Atlantic Tropical Experiment Microwave Radiation Convective Clouds	Unclassified - Unlimited

19. Security Classif. (of this report)	20. Security Classif. (of this page)	21. No. of Pages	22. Price*
Unclassified	Unclassified	69	

*For sale by the Clearinghouse for Federal Scientific and Technical Information
Springfield, Virginia 22151

ACKNOWLEDGEMENTS

The authors would like to express their deep appreciation to Dr. Thomas T. Wilheit, Jr. of Goddard Space Flight Center for his technical guidance and cooperation on all phases of the program. They would also like to thank Dr. Kenneth R. Hardy of Environmental Research & Technology, Inc. for his advice and assistance in the interpretation of the radar data and the cloud dynamics.

TABLE OF CONTENTS

	Page
LIST OF ILLUSTRATIONS	ix
LIST OF TABLES	xi
1. INTRODUCTION	1
1.1 Purpose of Objectives of Study	1
1.2 Background	2
2. THE EXPERIMENT AND ANALYSIS APPROACH	7
2.1 The Radiometric Sensors and Related Data Sources	7
2.1.1 The Scanning Microwave Radiometer	7
2.1.2 The Radar System	8
2.1.3 Other Data Sets	11
2.2 The Analysis Approach	12
2.3 The Empirically Derived Brightness Temperature - Rain Rate Relationship	14
3. PRECIPITATION IN CONVECTIVE CLOUD MASSES - 2 SEPTEMBER 1974	19
3.1 The General Synoptic Situation	20
3.2 Microwave Measurements of a Twin-Celled Cloud Mass	30
3.3 Microwave Measurements of Cloud Mass Collision	39
4. THE EFFECTS OF PRECIPITATION ON SATELLITE MICROWAVE MEASUREMENTS	49
5. CONCLUSIONS AND RECOMMENDATIONS	55
REFERENCES	57

LIST OF ILLUSTRATIONS

Figure		Page
1-1	Comparison of Brightness Temperatures for 19.35 Ghz Computed for a 4 km Uniform Rainfall Marshall-Palmer Cloud	3
1-2	Brightness Temperature for 19.35 GHz at a Viewing Angle of 45 Degrees	6
2-1	GATE Experiment B-Scale and C-Scale Area	9
2-2	Means and Standard Deviations of Brightness Temperature Derived from GATE Aircraft ESMR Data as a Function of Rain Rate	15
2-3	The Relationship between Brightness Temperature and Rain Rate as Derived from GATE Aircraft ESMR Data	17
3-1	Surface Streamline Analysis for 1200 GMT, 2 September 1974	21
3-2	Surface Streamline Analysis for 1800 GMT, 2 September 1974	22
3-3	850 mb Streamline Analysis for 1200 GMT, 2 September 1974	23
3-4	850 mb Streamline Analysis for 1800 GMT, 2 September 1974	24
3-5	SMS Visible Imagery (1/2 mi. resolution) for 1200 GMT, 2 September 1974	25
3-6	SMS Visible Imagery (1/2 mi. resolution) 1400 GMT, 2 September 1974	26
3-7	Radar Images along the NASA CV-990 Flight Line Taken from the Oceanographer from 1200 to 1530 GMT, 2 September 1974	27
3-8	Microwave Imagery of the Twin-Celled Cloud Mass at 1237 GMT, 2 September 1974	34

LIST OF ILLUSTRATIONS (Continued)

Figure		Page
3-9	Microwave Imagery of the Twin-Celled Cloud Mass at 1247 GMT, 2 September 1974	35
3-10	Microwave Imagery of the Twin-Celled Cloud Mass at 1322 GMT, 2 September 1974	36
3-11	Microwave Imagery of the Tip of a Cloud Mass at 1422 GMT, 2 September 1974	41
3-12	Microwave Imagery of the Tip of a Cloud Mass at 1439 GMT, 2 September 1974	42
3-13	Microwave Imagery of the Tip of a Cloud Mass, a Cloud Line and a Cumulus Congestus at 1456 GMT, 2 September 1974	43
3-14	Microwave Imagery of the Combined Cloud Mass, Cloud Line and Cumulus Congestus System at 1520 GMT, 2 September 1974	44
3-15	Radar Imagery of the Combined Cloud Mass, Cloud Line and Cumulus Congestus System	46
4-1	Nimbus 5 Microwave Imagery of the GATE Area at 1300 GMT, 2 September 1974	50
4-2	Radar Imagery of the GATE Area at 1300 GMT, 2 September 1974	51

LIST OF TABLES

Table	Title	Page
2-1	Radar Grey Scale Threshold	10
3-1	NASA CV-990 Measurement Runs MISSION 245-1, 2 September 1974	31
3-2	Microwave Grey Scale Categories	33

1. INTRODUCTION

1.1 Purpose and Objectives of Study

During the summer of 1974, the Global Atmospheric Research Program (GARP) sponsored an intensive investigation of the tropical zone extending from Africa across the Atlantic Ocean to South and Central America. This experiment, known as the GARP Atlantic Tropical Experiment (GATE), was designed to collect detailed meteorological and oceanographic data which would permit a better understanding of tropical meteorology and the role of the tropics in the general circulation of the earth's atmosphere. As part of this program, microwave and radar measurements were made of precipitation, a parameter of great importance as an indicator of the amount and distribution of latent heat release, the upward mass flux and the spatial organization of convection.

The derivation of rainfall rates from radiometric measurements requires a thorough understanding of the interaction of precipitation-size drops and centimeter wavelength radiation. In the case of active sensors, such as radars, this relationship is reasonably well-defined by a number of empirically derived equations relating reflectivity to rain rate. Relationships have also been derived for passive microwave radiometers using both theoretical and empirical approaches, but discrepancies between simulated and observed values have indicated the necessity for further research.

This report presents the results of a program which analyzed the radiometric data collected during GATE to study empirically the relationship between microwave measurements and rain rate in the tropics and to determine the characteristics of tropical precipitation. In this study, the 19.35 GHz (1.55 cm) microwave measurements made by a scanning radiometer flown on the NASA Convair 990 (CV-990) aircraft were compared with the rain rates indicated by a shipborne C-band (5.3 cm) radar mounted on the OCEANOGRAPHER to determine the effects of rain rate, sensor field of view and other parameters on total brightness temperature. The derived brightness temperature-rain rate relationship was shown to agree well with that predicted by microwave theory, and to be applicable to satellite measurements when inferring spatially averaged rainfall.

The relationship between microwave measurements and precipitation was then used with the GATE aircraft data to study the horizontal structure of precipitating systems. Two cases were studied; in the first a cloud mass consisting of two independent cumulonimbi achieved a steady-state system with heavy rainfall; in the second case there was an apparent merger among three clouds which proceeded to develop explosively and then to dissipate rapidly. Section 2 discusses the derivation of the microwave-precipitation relationship; Section 3 presents the case analyses of GATE data; Section 4 summarizes the implications for satellite rainfall mapping; and Section 5 includes the conclusions and recommendations.

1.2 Background

The determination of the effects of precipitation upon microwave radiation has been the subject of a number of theoretical studies and empirical analyses since precipitation-size drops are the primary contributors to nonresonant opacity in the microwave region. Raindrops contribute strongly to absorption and scattering of microwave radiation, and thus it is natural to suppose that information about precipitation may be inferred directly from microwave measurements. Furthermore, since rain rate at the earth's surface is the standard synoptic parameter used to identify and measure precipitation, it is desirable to derive direct relationships between brightness temperature (T_B) and rain rate.

One approach to the derivation of such relationships has been to simulate the effect of precipitation-size droplets on microwave radiation through the use of Mie scattering theory and the equation of radiative transfer. This approach, requiring the iterative solution of computationally complex scattering functions and interaction models, was used by Wilheit et al (1975) with a uniform rain cloud extending from the melting level of the atmosphere to the ocean's surface and characterized by Marshall-Palmer drop-size distribution (Marshall and Palmer, 1948). Their findings, shown in Figure 1-1 for the 4 km melting level and the frequency of 19.35 GHz, showed that rain less than 1 mm hr^{-1} has little effect on the total emission and that rain rates greater than 20 mm hr^{-1} saturate the emission values. Between these limits, the

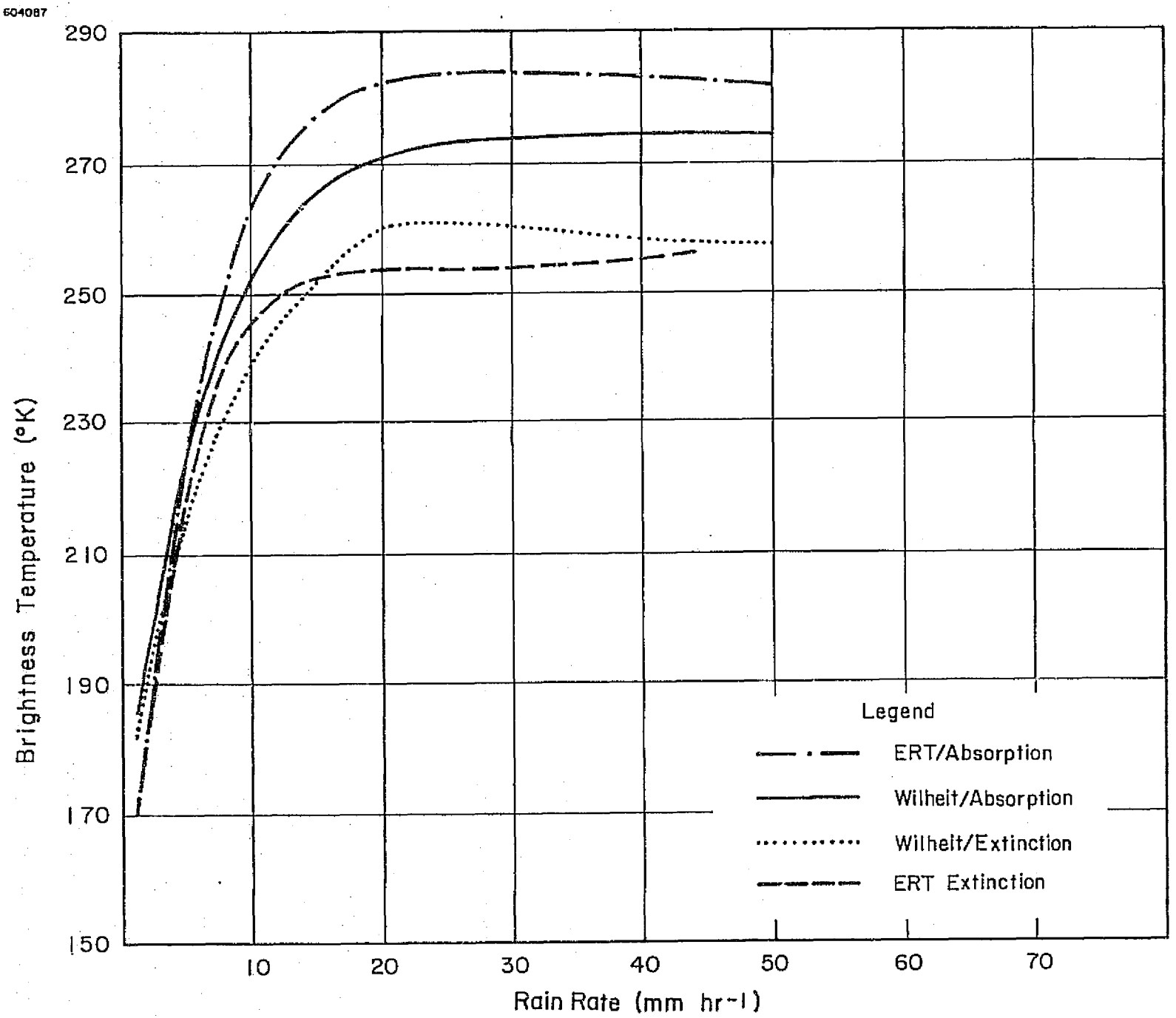

Figure 1-1 Comparison of Brightness Temperatures for 19.35 GHz Computed for a 4 km Uniform Rainfall Marshall-Palmer Cloud using Full Mie Scattering Theory and no Scattering (Wilheit et al, 1975) and the ERT Model for Scattering and no Scattering (Fowler et al, 1976)

sharp increase in brightness temperature with rain rate permits reliable discrimination of rainfall amounts using microwave measurements.

The effect of scattering by raindrops is also evident in Figure 1-1 by comparison of the curves labeled "Wilheit/Absorption" and "Wilheit/Extinction", the latter curve representing absorption plus scattering effects. Scattering due primarily to millimeter-size drops tends to decrease the total emission such that the measured values remain colder than the temperature of the top of the rain layer, 273°K. On the other hand, without scattering, that is, without a number of large drops, the measurements become asymptotic to the physical temperature of the raindrops. One implication of this effect is that a rain rate which is characterized by a drop-size distribution of mostly small drops should appear warmer than that which is characterized by a distribution of large drops which leads to significant amounts of scattering.

Using an approximation to both the scattering function and the equation of radiative transfer, Fowler et al (1976) performed similar calculations on the cloud model used by Wilheit and the results are given by the curves labeled "ERT" in Figure 1-1. These curves show the same qualitative relationships as those found by Wilheit et al (1975) while differing slightly in quantitative value, since even at very high rain rates the ERT model showed some contribution to emission from layers below melting level. Their study also investigated types of drop-size distributions, vertical cloud structures and atmospheric temperature structures representative of the natural variability in global weather. Variations in the atmospheric temperature structure were shown to have the largest effect on the relationship between brightness temperature and rain rate, eliminating the possibility of a universally applicable algorithm. This agreed with the analysis of the effects of changes in height of the melting level given by Wilheit et al (1975). During the GATE experiment, variation in atmospheric structure were of minimal importance, since all data was collected in the tropics under relatively uniform atmospheric conditions. It should be noted, however, that the analysis presented below is thus probably applicable only to the tropics.

Changes in cloud structure (e.g., variations in rain rate and drop size with height) also caused significant (10° to 20°K) changes in the

brightness temperature associated with a given surface rainfall rate. Nevertheless, because of the sharp response of T_B to rainfall rate changes, the rain rate over a fairly large range could be inferred from the differing cloud T_B's with an error as small as 2 mm hr^{-1}. Even less error was caused by variations in the drop-size distributions of the surface rainfall layer, since both the amount of microwave emission and the measured rain rate are highly correlated with the number of large drops present.

Experimental measurements of brightness temperature versus rain rate have supported the theoretically predicted relationships. Figure 1-2 (Wilheit et al, 1975) shows that the ground-based data agrees very well with theoretical computations, although slightly higher values are indicated in theory for high rain rates. Compared with the theoretical models, satellite measurements representing a very large field of view differ more, although generally allowing inference of rain rates within 2 mm hr^{-1} accuracy. However, other work such as that done by Sabatini et al (1975), comparing satellite microwave and radar measurements, has indicated substantially different rain rate relationships with maximum brightness temperatures of 220°K. Most of the differences can probably be attributed to areal averaging across the beam and to partially filled fields of view, but further research is needed to resolve completely the discrepancies.

One of the goals of this study was to use data collected during the GATE experiment to investigate further the relationships discussed above and the questions that have been raised by various authors. During this experiment, the aircraft ESMR radiometer operating at a frequency of 19.35 GHz was carried by NASA's CV-990 aircraft to provide high resolution maps of rain cells in an area also mapped at varying altitudes by a horizontally scanning shipborne radar. Microwave measurements from the satellite-borne ESMR radiometer, operating at 19.35 GHz, were also available for the same region. It was hoped that through the use of these radiometric data sets, the effects of rain upon microwave measurements could be empirically determined. As discussed below, this goal was met, though with somewhat limited success due to lack of resolution in the radar data.

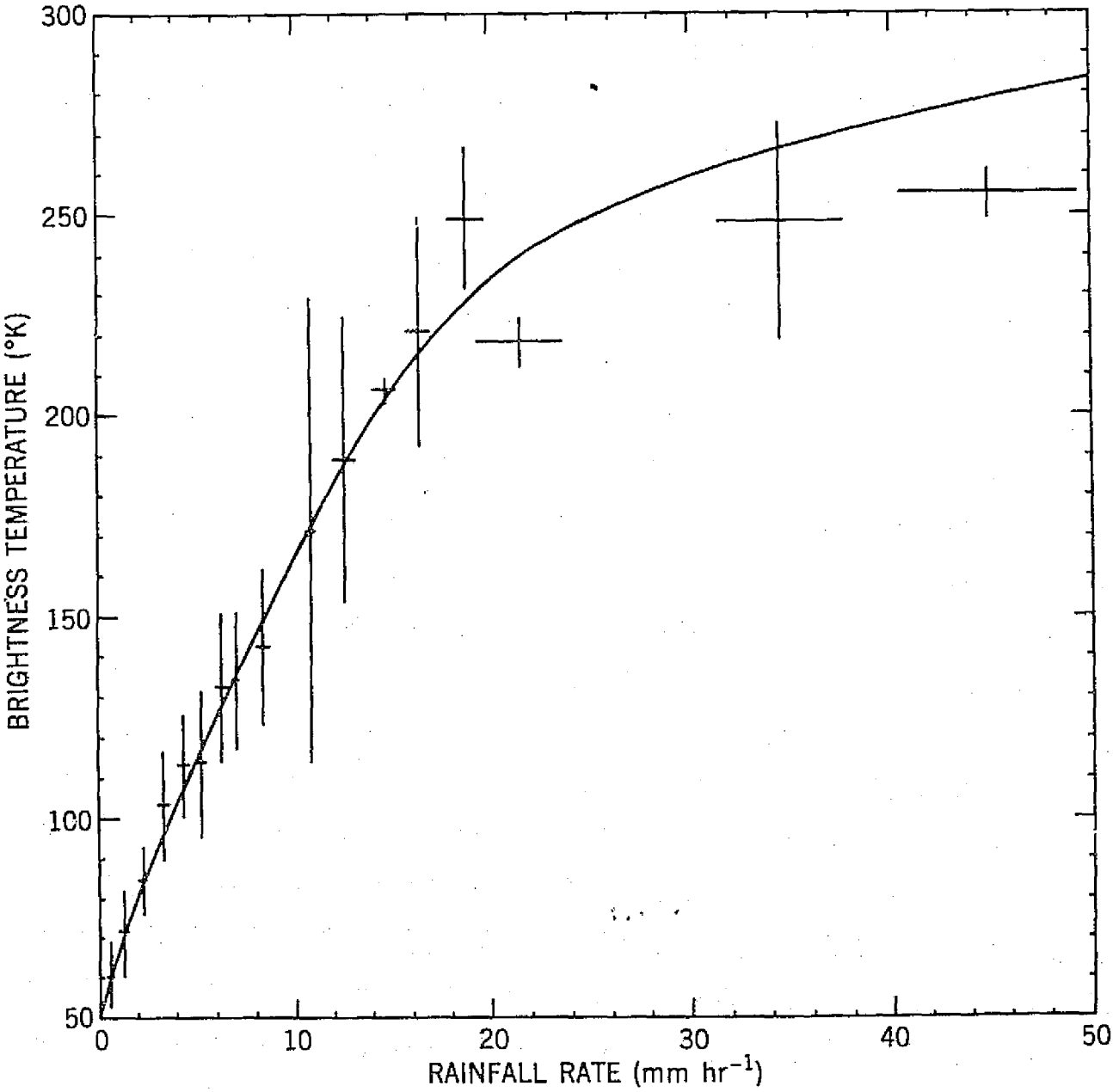

At each point, the height and width of the cross represent two standard deviations in the corresponding dimensions. The solid line is the theoretically calculated curve.

Figure 1-2 Brightness Temperature for 19.35 GHz at a Viewing Angle of 45° with respect to the Zenith as a Function of Directly Measured Rain Rate

609125

2. THE EXPERIMENT AND ANALYSIS APPROACH

2.1 The Radiometric Sensors and Related Data Sources

2.1.1 The Scanning Microwave Radiometer

The Electrically Scanning Microwave Radiometer (ESMR) flown on NASA's CV-990 was a passive radiometer operating at a frequency of 19.35 GHz (1.55 cm wavelength) with horizontal polarization and a 2.85° x 2.85° beam width. As the aircraft flew along a flight path, the radiometer scanned from 50° to the left of nadir, to nadir, then to 50° to the right of nadir in 39 steps every two seconds. At the end of each scan the instrument viewed alternately either a warm (320°K) or a cold (77°K) load for calibration purposes. At the normal experimental altitudes of 9 to 12 km, this meant that an area approximately 18 to 28 km wide along the flight path was sampled every two seconds with enough data resolution to identify individual precipitation cells. An oscilloscope displaying the uncalibrated signal permitted real-time qualitative assessment of precipitation intensity and its changes with time and space, while a magnetic tape recorder saved all data for post-flight analysis.

Post-experiment data processing converted the measured emissions to microwave brightness temperature maps and to color-coded brightness temperature range maps. In the processing, the brightness temperatures were corrected for scan angle effects (increased path length through the atmosphere) so that the brightness temperatures were adjusted to the equivalent nadir value and could be compared horizontally. In this study the color-coded brightness maps were used as a guide to identify precipitation areas encountered during the experiment. The detailed analysis was based upon the actual brightness temperature measured at each scan spot and given in digital maps. To supplement these measurements, the in-flight qualitative precipitation analyses were used in conjunction with the meteorological observations made by an observer with the ESMR system and by the official aircraft observer.

2.1.2 The Radar System

The radar observations of clouds and precipitation discussed in this report were made from the OCEANOGRAPHER, the ship located at the southeastern point of the C-scale area (see Figure 2-1, ship 4, USA) during September, 1974. Mounted on this ship was a C-band (5.3 cm) radar belonging to the National Oceanographic and Atmospheric Administration (NOAA), which scanned horizontally at selected elevation angles to provide reflectivity values corresponding to the spatial and temporal distribution of hydrometeors. The principal characteristics of this system and its measurements have been summarized in the GATE data documentation by Hudlow (1975).

Reflectivity measurements using this radar were made on a continuous basis throughout the entire GATE experiment. These values were recorded digitally every 15 minutes but were not available for use at the time of this study. Instead the data base consisted of 16 mm film containing grey scale maps of rain rate at five minute intervals. These maps were made by photographing a scope which displayed day, time and antenna tilt angle (0° to 22°) as well as six intensity levels delineated by isoecho contours. These contours were derived from an analog video integrator and processor (AVIP) which was designed to average over range and azimuth and to sense six integrated video threshold levels. As a result, the grey scale maps show values averaged over 2° azimuth intervals and 1.85 km range increments across a range of 18.5 km (10 n.mi.) from the ship out to 233 km (125 n.mi.). All of these values are range-normalized to a range of 233 km.

The grey scale values on the microfilm correspond to the reflectivity factors and rain rate threshold values shown in Table 2-1, taken from Hudlow (1975).

Phase 3 (30 Aug. - 19 Sept. 1974)

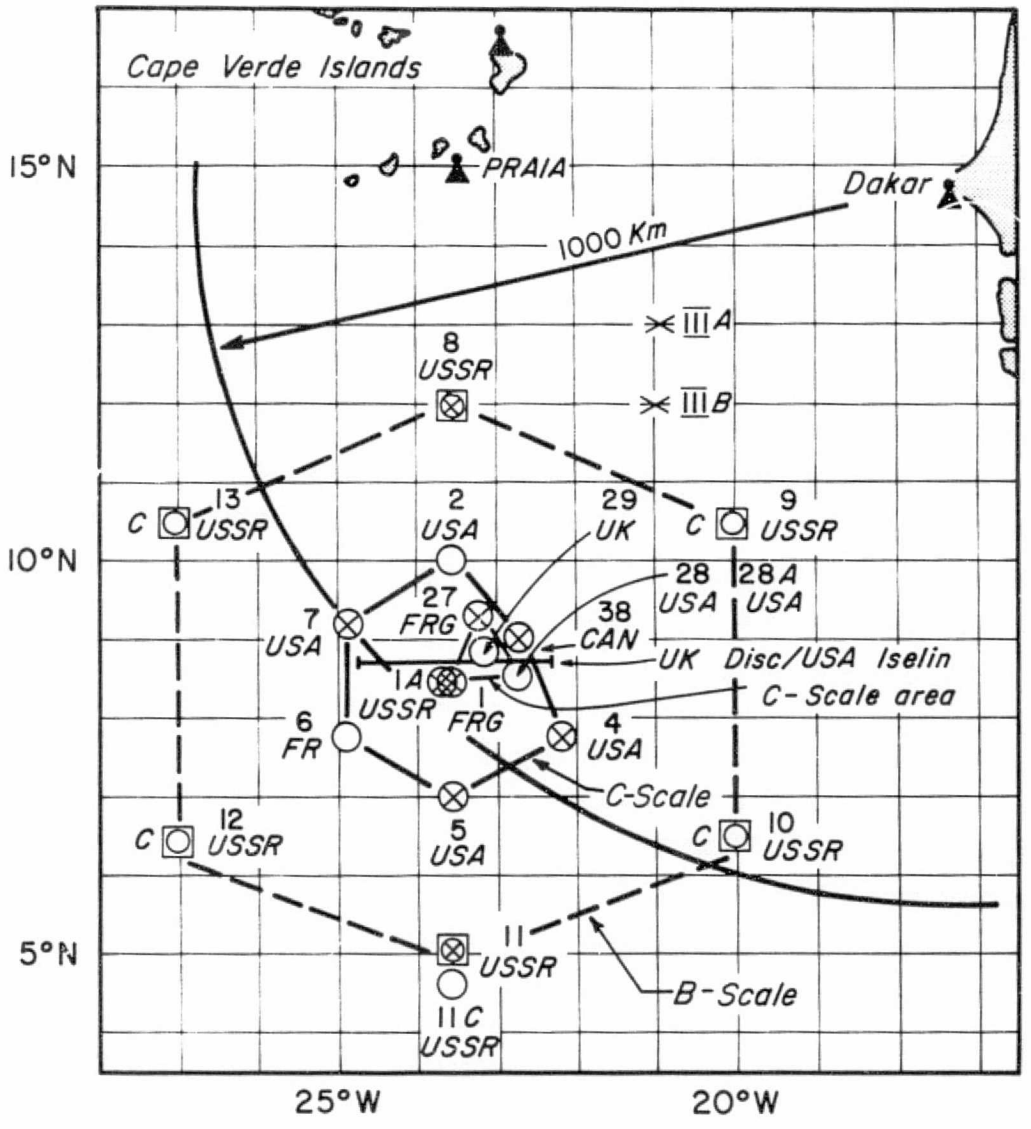

KEY

- ○ B – Scale ship-position
- ⊗ B – Scale radar ship-position
- ◎ A/B – Scale ship-position
- ⊠ A/B – Scale radar ship-position
- C Communications ship
- ▲ Station – position Radiowind/Radiosonde
- ⋊ Intercomparison Point
- ⊢ Roving oceanographic ship

Figure 2-1 GATE Experiment B-scale and C-scale Area

605033

TABLE 2-1

RADAR GREY SCALE THRESHHOLDS

Color	Level	Reflectivity Factor (dbz)	Rain Rate (mm hr^{-1})
Black	-	No Echo	-
Grey	1	Variable	Variable
White	2	28	1.6
Black	3	36	7.0
Grey	4	44	30.5
White	5	52	133.3
Black	6	60	581.7

In Table 2-1, dbz corresponds to 10 log Z where Z has units of ($mm^6\ m^{-3}$) and the rain rate (R) is derived using the relationship $Z = 350\ R^{1.25}$.

As can be seen from the above discussion, the radar data set covers a far greater area and time period than does the microwave sensor but provides values at a far coarser resolution in time, space and precision. This is not due to any inherent limitations in the radar system but rather limitations in data availability at the time of this analysis. However, the radar data set does permit a good evaluation of the vertical and horizontal structure of precipitation and cloudiness and permits qualitative comparison with the microwave measurements when both are coincident in time and space.

2.1.3 Other Data Sets

Since radiometric measurements are influenced both by the precipitation and the atmosphere, certain other data sets were used in conjunction with the microwave and radar measurements. These data sets included the standard hourly surface observations made from the ships in the B-scale area and the radiosonde soundings made every six hours at the same locations to permit an analysis of the synoptic conditions in the experiment area. Additional information was supplied by the in situ meteorological measurements made by the CV-990 and by the infrared temperature measured from the aircraft by a downlooking radiometer in the 9.5 to 11.5 μm atmospheric window. This latter sensor provided cloud top or surface temperatures every ten seconds along the flight path at nadir.

Satellite data were employed to assess the large-scale temporal and spatial cloud characteristics. In particular the 4 and 2 n.mi. resolution infrared and 1/2 n.mi. visible photographs taken from the Synchronous Meteorological Satellite (SMS) every thirty minutes were used to study the diurnal variability of cloudiness over the GATE area. Microwave brightness temperatures made by the Nimbus-5 ESMR system at the time of passage over the GATE area (∿ 1130 GMT) were also analyzed to determine the effect of spatial averaging on the inference of rain rates from satellite.

2.2 The Analysis Approach

To investigate the relationship between microwave radiation and precipitation, a search through the NASA CV-990 aircraft ESMR data set was made for missions with a significant amount of precipitation indicated on the microwave maps. These missions were then compared with the available radar data sets to identify days and regions for which coincident measurements were available. As the result of this selection process, two cases were chosen: (1) 2 September 1974, an Intertropical Convergence Zone (ITCZ) line study; and (2) 5 September 1974, a cloud cluster study. Both of these days were characterized by a considerable number of convective cells with precipitation of varying intensity and by multiple measurements of the same cells over a several hour period. In addition, detailed notes by an observer flying with the aircraft ESMR system were available to supplement the standard cloud observations.

Comparison of the aircraft microwave measurements and the ship-based radar measurements was made through the use of digital brightness temperature maps supplied by NASA/GSFC and grey scale reflectivity maps supplied by the NOAA World Data Center A. Since the two data sets were taken by instruments which differed significantly in resolution and position relative to the rain cells, the first phase of the analysis concentrated on identifying the individual rain cells and determining the location of each cell. Microwave maps were analyzed in 25°K temperature intervals to locate regions of high brightness temperature indicative of areas of precipitation. The position of each region, identified in the data set by time, was then determined through the use of the NASA CV-990 flight records and checked against the in-flight observations of precipitation and cloud conditions.

The position of the same cells on the radar microfilm was determined through the use of recorded azimuth angle and range markings. To verify these positions, the locations of the selected cells and those of surrounding cells were compared with visual observations of the cloud patterns near the flight path. The vertical structure of each cell was also derived through the use of radar observations at varying elevation angles and checked against visual observations of cloud height and cloud type.

Figures 3-14 and 3-15 (to be discussed in detail in Section 3) show one such precipitation area as mapped by the microwave radiometer and by the radar, respectively, with the similarities and differences in the two data sets clearly evident. First, the high resolution microwave data (see Figure 3-14) reveals a considerable amount of cloud and cell structure in the horizontal which is not seen in the lower resolution radar observations (see Figure 3-15). Along the longitude band from 9°06'N to 9°27'N, a number of cells of varying brightness temperature values and clearly identifiable shapes can be located within the microwave map. In the coarse radar data, however, these cells appear as one very large cell characterized by heavy precipitation from 9°07'N to 9°25'N. Qualitatively, the location of the heavy precipitation observed with the radar agrees well with the band of high brightness temperatures, but the detailed spatial variability indicated by the microwave data is missing in the radar observations.

Another aspect of the radar data which eliminates much of the structure in the precipitation measurements is the large range in rain rates represented by each grey scale. Previous microwave studies (see Figure 1-1) have indicated that brightness temperatures increase from 180° to 230°K as rain rates increase from 1 to 7 mm hr^{-1} and that the temperatures reach their maximum values by 20 mm hr^{-1} rain rate. With two radar grey scales representing this entire range in rain rates (1 to 7 mm hr^{-1}, 7 to 30 mm hr^{-1}) almost all of the natural variability in precipitation and the measured variability in microwave data is lost. Thus, not only do the radar and microwave differ in spatial resolution, they also differ in measurement sensitivity.

These two resolution differences, the spatial resolution and the rain intensity resolution, were the cause of the major difficulties encountered in quantitatively comparing the microwave and radar measurements and in using the radar-indicated rain rates to derive brightness temperature and rain rate relationships. It was not possible to obtain exact rain rates over an area because of the grey scale categories, nor was it possible to identify the locations of transition from one grey scale to the next with sufficient precision to correlate microwave measurements with the known boundary rain rates. Furthermore, study of several cells indicated that the integrated rain rate given by the radar

would be lower than rain rates occurring in many locations of the resolution element.

The approach used to minimize the effects of differing resolutions relied upon meteorological and radiometric analysis and was, of necessity, somewhat subjective. Each precipitating mass which appeared in both the microwave and radar imagery was carefully analyzed in terms of its width, height, precipitation structure and stage of development. This analysis was based not only upon individual radiometric maps but also upon the time sequences of the cells as indicated by radar and multiple aircraft passes, and upon visual cloud observations made during flight.

Using the analyzed cloud conditions as a guide, rain rate values were estimated for areas within each grey scale category shown on the radar imagery. For the lowest grey scale, indicating values of less than 1.6 mm hr^{-1}, rain rates were estimated simply by spatially interpolating from the edge of the cloud to the next grey scale category. In the case of a cloud where only light rain was indicated by the radar, but analysis indicated some structure, a value of 1.6 mm hr^{-1} was assumed to apply to the cloud center. A similar approach was used to assign values of 1.6, 4 or 7 mm hr^{-1} to the second level, 7, 10 or 20 mm hr^{-1} to the third level and 30 mm hr^{-1} to the fourth level. For each estimated rain rate area within a cell, three contiguous brightness temperature values were then read from each scan line. With more than a dozen radar indicated cells available for analysis, approximately 1,000 microwave data points were obtained whose values represented the variety of microwave readings found for each radar averaged rainfall rate.

2.3 The Empirically Derived Brightness Temperature-Rain Rate Relationship

Figure 2-2 shows the brightness temperature means and standard deviations derived from the above data set for the selected rainfall rates. These show clearly expected trends in brightness temperature against rain rate. The mean increases sharply with rain rate up to 7 mm hr^{-1}, then becomes asymptotic at higher rain rates. Significantly large standard derivations are seen in the temperatures observed for low rain rates, reflecting both the physical effects of high rain rates

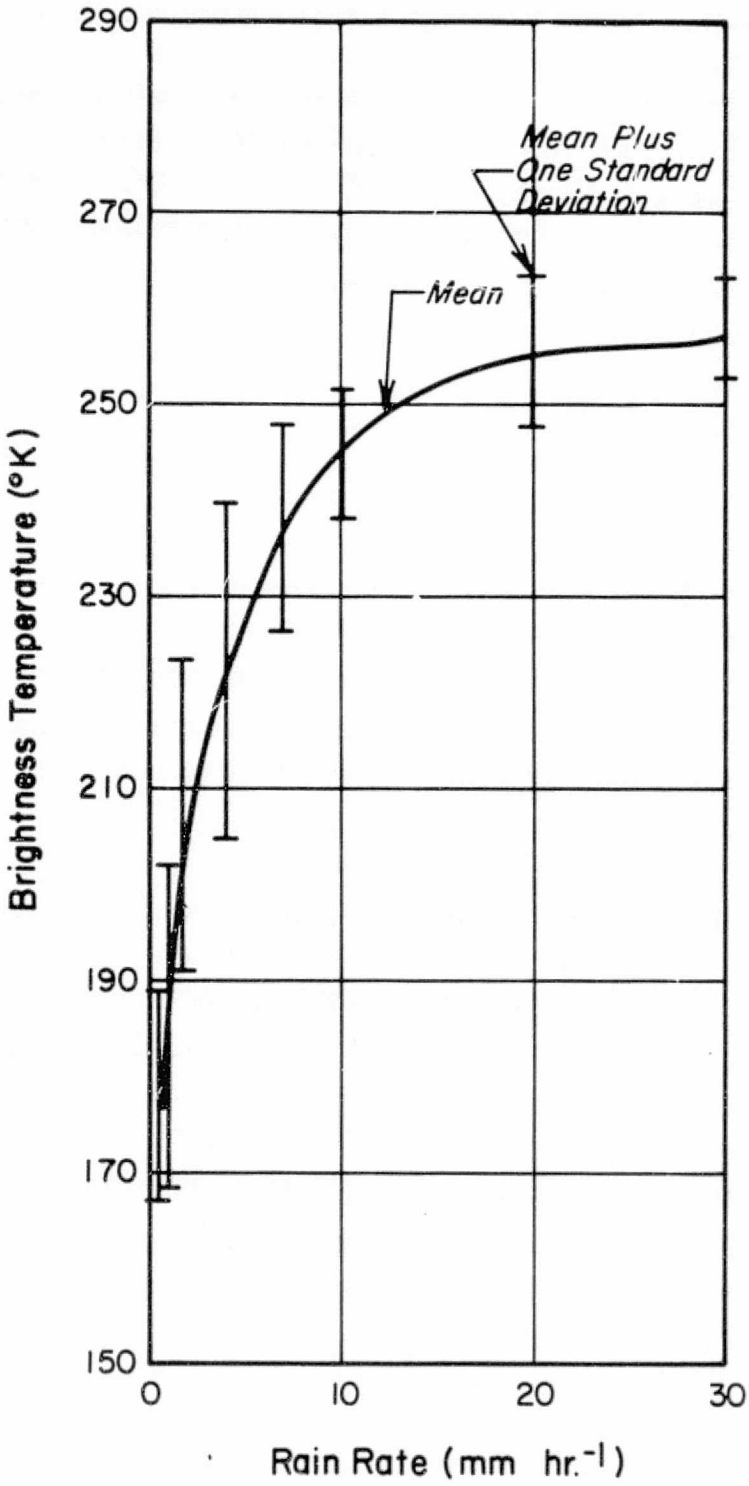

Figure 2-2 Means and Standard Deviations of Brightness Temperature Derived from GATE Aircraft ESMR Data as a Function of Rain Rate

imbedded in an area of average light rainfall, and the sharp radiometric response to small rain rate changes when the rain rate is less than 10 mm hr^{-1}.

The error bars are also correlated with the limits of the initial grey scale categories. Examination of the standard deviation maximum and minimum found for each rain rate showed that the observed brightness temperatures generally fell within the range of mean values for the appropriate radar echo levels. For example, the minimum value for the 7 mm hr^{-1} data set exceeded the mean for 1.6 mm hr^{-1} and the maximum value was less than the mean for 30 mm hr^{-1}. The only exceptions to this rule were the 4 mm hr^{-1} data set and the 10 mm hr^{-1} data set. These showed a few values which, in the first case, appear too high for the 1.6 to 7 mm hr^{-1} brightness temperature range and in the latter case appear too low for the 7 to 30 mm hr^{-1} range. Considering the various sources of error in the data set, such points are not surprising. Rather it is encouraging that, in general, the variability found in the data can be explained in terms of the rain rate estimation procedure, and that despite the variability the overall trends seem physically realistic.

The brightness temperature-rain rate relationship derived from a least squares fit to the data is shown in Figure 2-3 with the model and the theoretical relationships given by Wilheit et al (1975) and Fowler et al (1976). Comparison of the curves shows that the empirically derived relationship gives brightness temperatures which are slightly higher than expected from the theoretical relationship for rain rates up to 10 mm hr^{-1}; this leads to a 2 mm hr^{-1} difference in indicated rain rate values with the empirical curve predicting the lower rain rates. Both Wilheit et al (1975) and Fowler et al (1976) have predicted an error of that magnitude, the first group on the basis of measured values compared with theoretical and the second on the basis of the effects of differing cloud structure. Since the data set used did contain measurement errors, differing cloud conditions and uncertainties in the rainfall rate, such agreement between theory and observation is excellent.

For rain rates of 10 to 20 mm hr^{-1}, the empirical curve agrees very well with the theoretical predictions of Fowler et al (1976) even to indicating the point of inflection 15 mm hr^{-1}. Beyond 20 mm hr^{-1} the

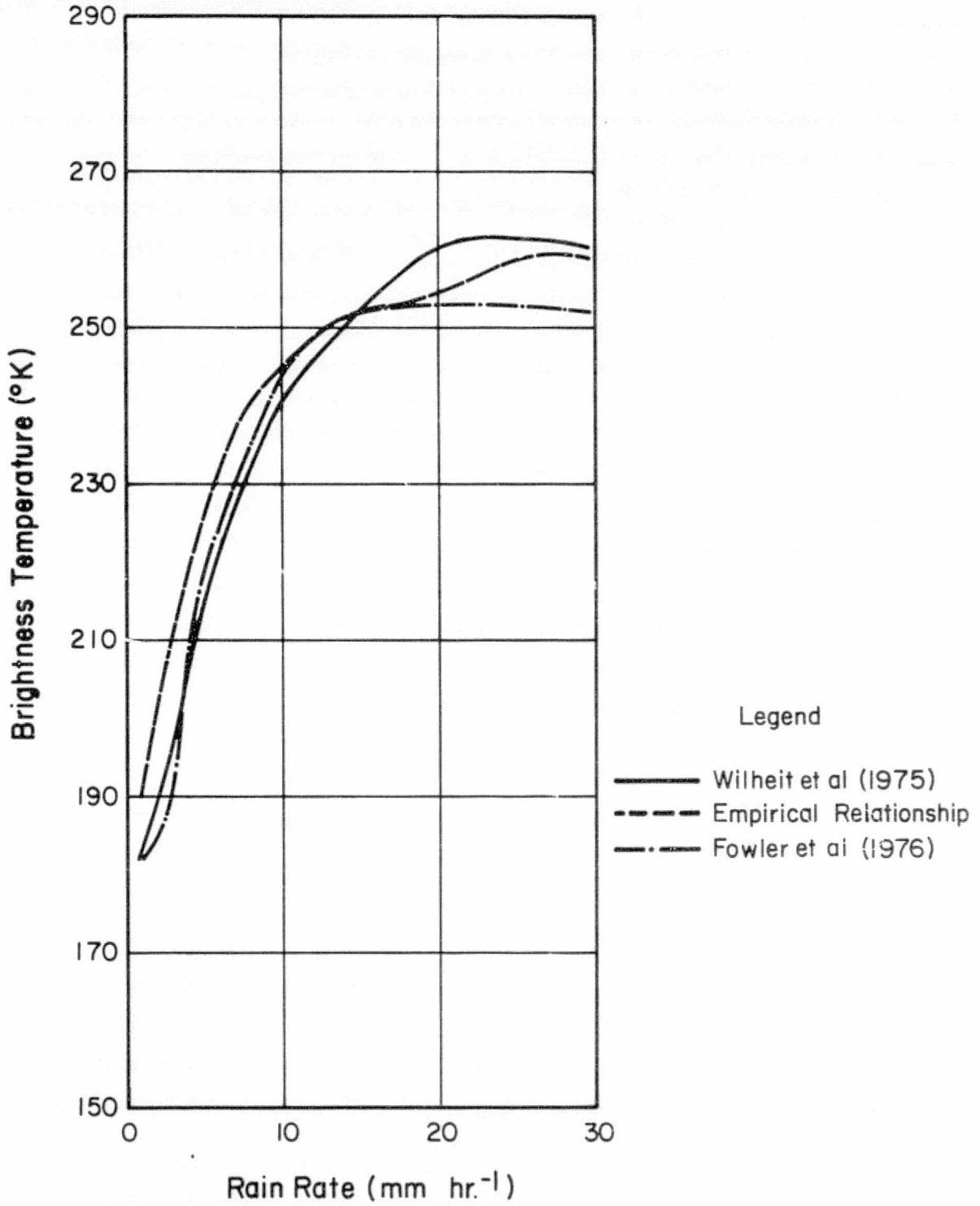

Figure 2-3 The Relationship between Brightness Temperature and Rain Rate as Derived from GATE Aircraft ESMR Data

shape of the empirically derived curve departs from both the mean data values and the theoretical values as the limited amount of data for the high rain rates precluded a good least squares fit. Reference to Figure 2-2 does show, though, that the mean measured values are higher than those predicted by Fowler et al (1976) and more closely approximate the values predicted by Wilheit et al (1975).

One of the questions raised in earlier studies is the exact upper limit of measured brightness temperatures, that is, do measurements of precipitation reach values of 273°K as absorption theory predicts for rain starting at the freezing level. A survey of the data values collected over the high rain rates showed that the majority of brightness temperatures did not exceed 265°K, well within the difference from extinction theory that would be due to system noise alone. A few higher readings were found with values up to 270°K, but these were too rare to invalidate the relationship shown in Figure 2-3. In fact, since they are associated with cloud structures significantly different from the rain model used in theoretical calculations, the lack of more substatial deviations tends to confirm the derived relationship.

Comparison of the GATE microwave and radar data thus confirms the theoretical predications of the effect of rain on centimeter wavelength radiation under tropical conditions. It also shows that the aircraft data should be useful for inferring rain rates up to 15 mm hr^{-1} with an accuracy of approximately 2 mm hr^{-1}. This approach was used in the next section to study the spatial and temporal characteristics of precipitation during GATE.

3. PRECIPITATION IN CONVECTIVE CLOUD MASSES - 2 SEPTEMBER 1974

One of the missions selected for an analysis of precipitation characteristics was GATE Mission 245-1, a mission whose objective was to investigate the convective activity of a cumulus line. During this mission, the NASA CV-990 flew a number of passes along a path perpendicular to the axis of an east-west cloud line, sampling precipitation both within the cumulus band and in nearby regions. The mission was especially interesting in that repetitive measurements were made of the growth and activity of a cloud mass north of the cloud line. This cloud mass was characterized by very intense rainfall of considerable duration and contrasted sharply with the shorter, less intense cells located in the cloud line. In fact, the cloud line selected for study disintegrated early in the experiment to become an area of variable convective activity.

Very early in the study of this case, it became apparent that the high resolution data collected by the ESMR system revealed a great deal of information not only about the rainfall rates, but also about the horizontal structure and organization of precipitating cells. Of particular interest was the information provided about the behavior of individual cells within larger storm systems. Over the years, the most intense convective cells and precipitation have often been observed to be associated with cumulonimbi which have merged to form a massive cumulonimbus or have organized in cloud masses or cloud lines (see, for example, Simpson et al, 1971, or Woodley and Simpson, 1972). In the larger cloud masses, the individual clouds have frequently been observed to retain their identities and even to enhance each other's growth. Because of resolution limitations in most of the existing data, however, it has been difficult to study the effects of cloud merger or the behavior and organization of systems formed by multiple clouds.

The microwave measurements made on 2 September 1974 provided considerable detail on the cellular structure of precipitation in cloud masses and cloud lines. Two cases will be discussed here, one in which a twin-celled cloud mass was observed during a two hour period, and the other in which three cloud masses merged into one large entity. The first provides observations of the behavior of two large cumulus congestus and the convective area located between them; the second shows the changes occurring when well-developed cloud systems intersect to form one massive cloud region.

3.1 The General Synoptic Situation

The convective activity found on 2 September 1974 was associated with a weak circulation pattern located between 5° and 10°N and 20° to 25°W. Figure 3-1 shows the surface analysis at 1200 GMT, the start time of the GATE mission. This indicates a very weak trough stretching from 7°N, 25°W to 9°N, 20°W, then curving northeastward. The trough is evident also in the 1800 GMT chart (Figure 3-2). The inflow area for the convective activity was located near the 850 mb level at 1200 GMT with weak circulation suggested east of 25° and convergence evident west of 30°W (Figure 3-3). Although the circulation is not pronounced at noon, it is indicated by the col point (area of no wind) at 5°N, 24°W (Figure 3-3). The circulation has become quite evident by 1800 GMT (Figure 3-4).

Figures 3-5 and 3-6, the SMS visible images (1/2 n.mi. resolution) for 1200 and 1400 GMT, respectively, show the cloudiness associated with this circulation, and a growing cloud mass to the east. A very well-defined cloud line is found in the 1200 GMT imagery (point C) crossed by the flight path (line A) near its western end. By 1400 GMT, this cloud line has disappeared to be replaced by a region of disorganized cumulus activity and significantly increased cirriform cloudiness. At the northern end of the flight lines, though, cloud masses are evident in both images (points D and C, respectively) indicating a favored area for organized convective activity.

Radar data taken from the OCEANOGRAPHER (located at point B in Figures 3-5 and 3-6) during the period of the experiment provides an excellent history of the areal precipitation, and is summarized in Figure 3-7 showing the images sensed for the flight track area every fifteen minutes from 1200 GMT to 1530 GMT. In these images the white cells correspond to grey scale one (0 to 1.6 mm hr^{-1}), the black to grey scale two (1.6 to 7 mm hr^{-1}), and the white enclosed by black to grey scale three (7 to 30.5 mm hr^{-1}). The boxes shown on these images correspond to the approximate area and time on the microwave measurements. The latitude is given in degrees North while the ship's position is marked by a triangle. Comparison of the 1200 GMT radar image to the 1200 GMT satellite image shows that the cumulus line east of the flight track appeared as an elongated rain band and that light rain cells were

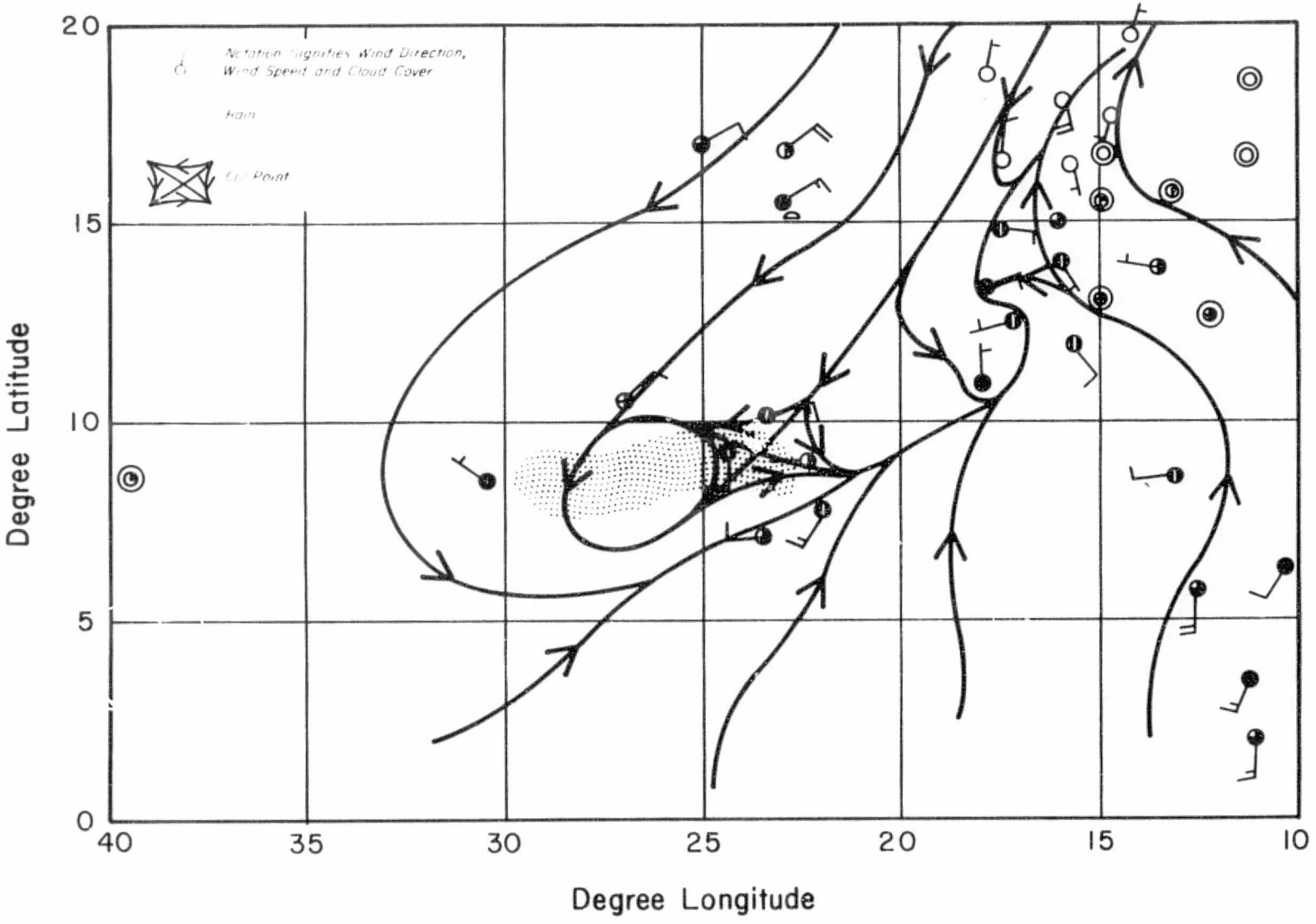

Figure 3-1 Surface Streamline Analysis for 1200 GMT, 2 September 1974

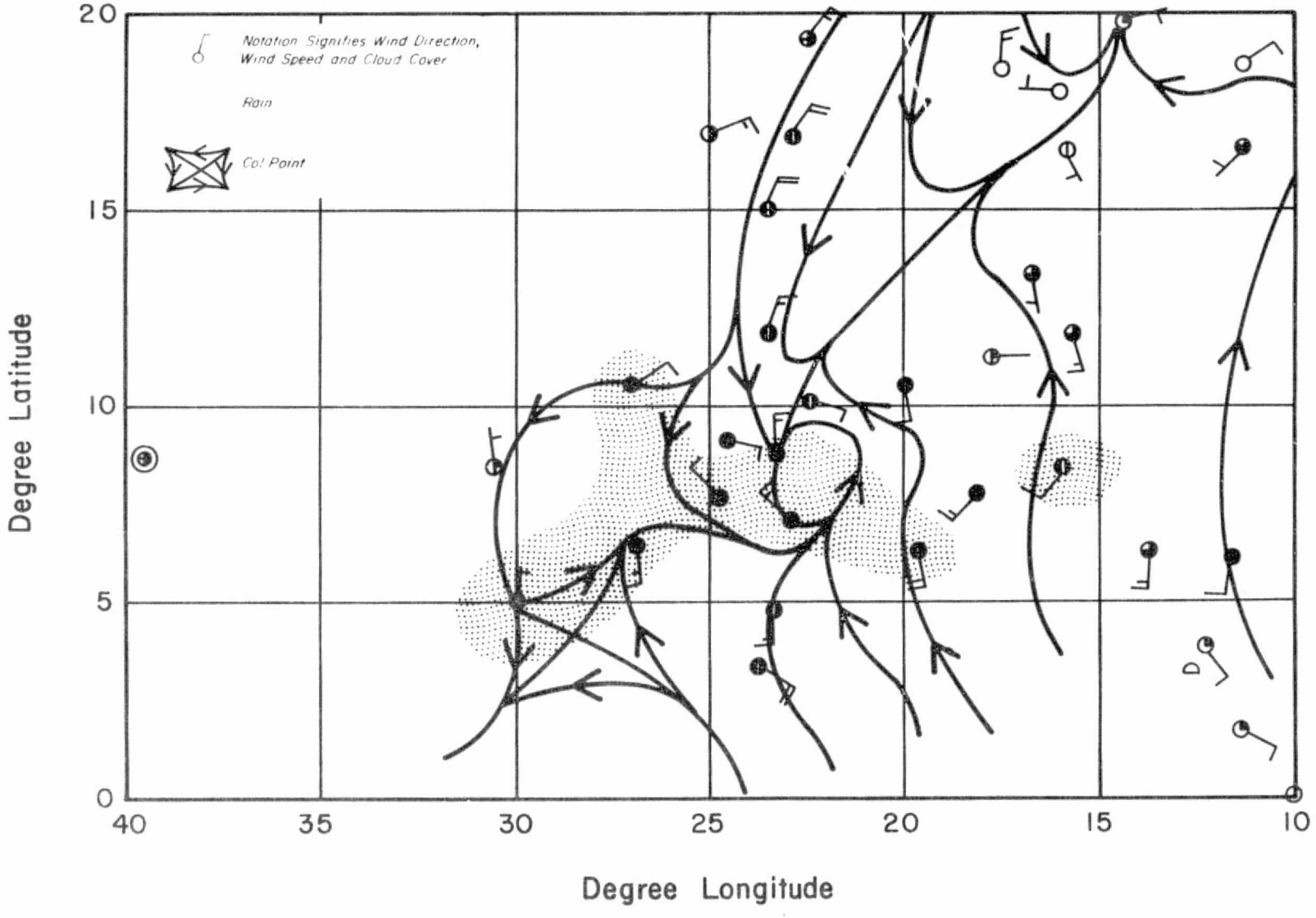

Figure 3-2 Surface Streamline Analysis for 1800 GMT, 2 September 1974

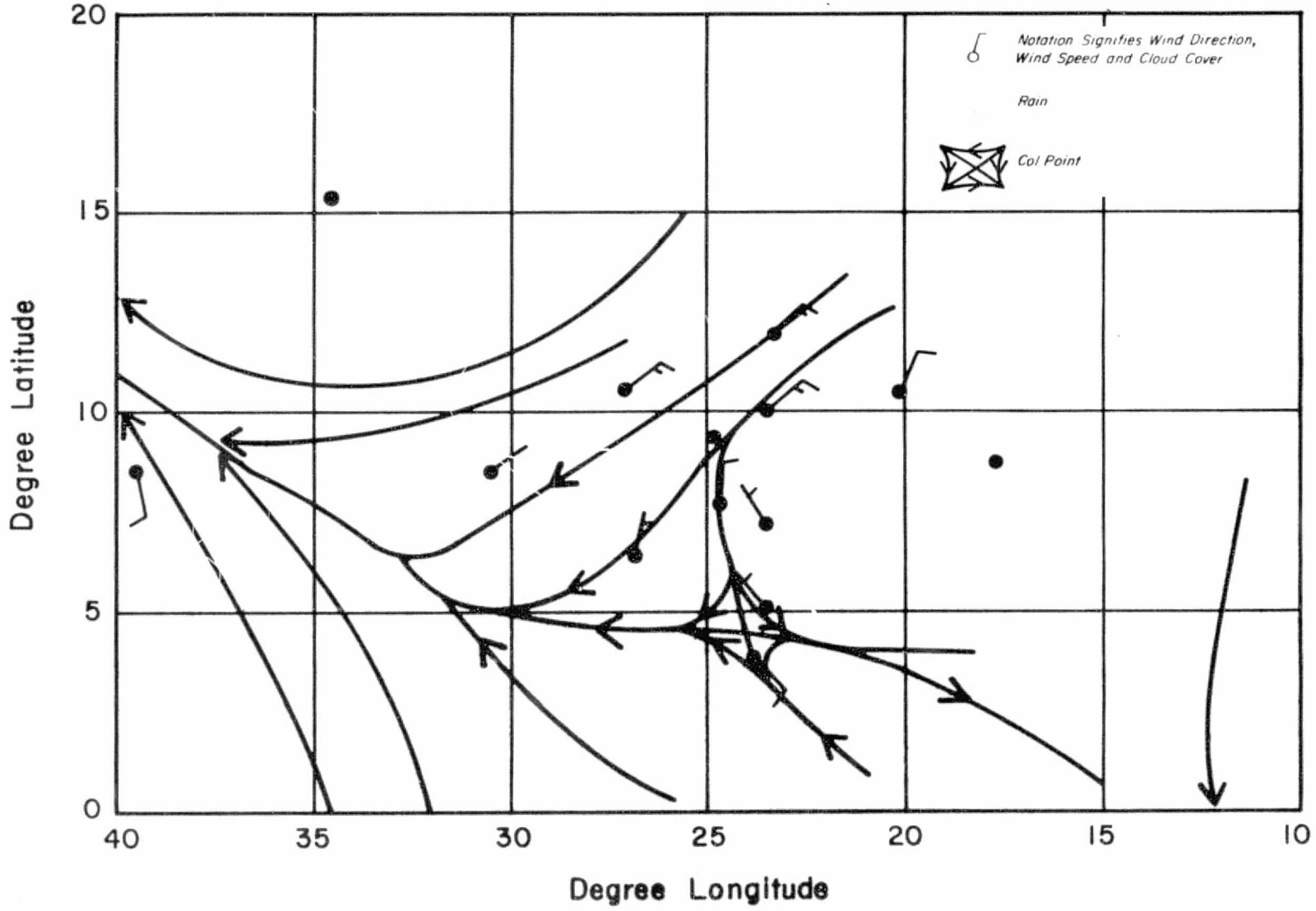

Figure 3-3 850 mb Streamline Analysis for 1200 GMT, 2 September 1974

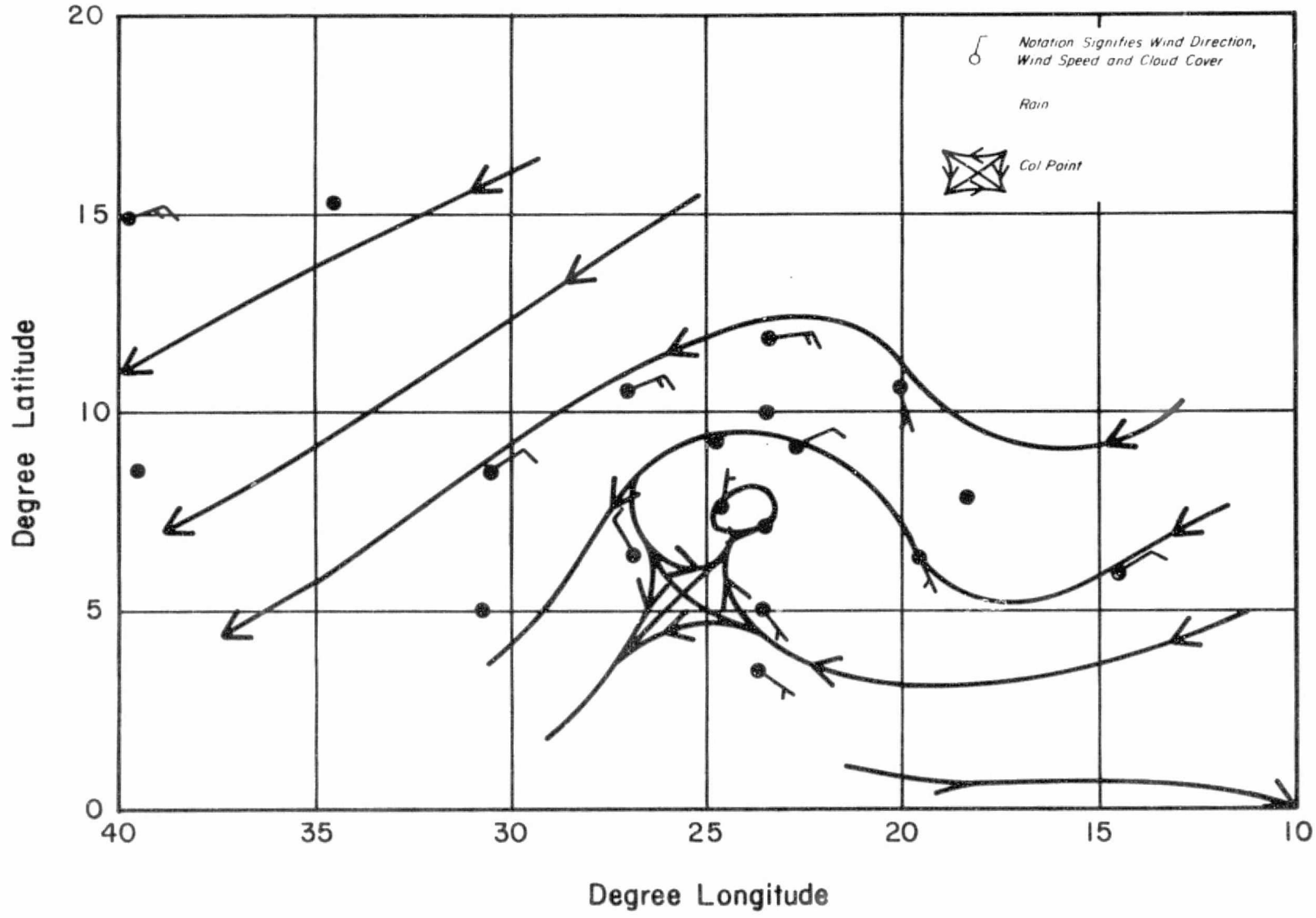

Figure 3-4 850 mb Streamline Analysis for 1800 GMT, 2 September 1974

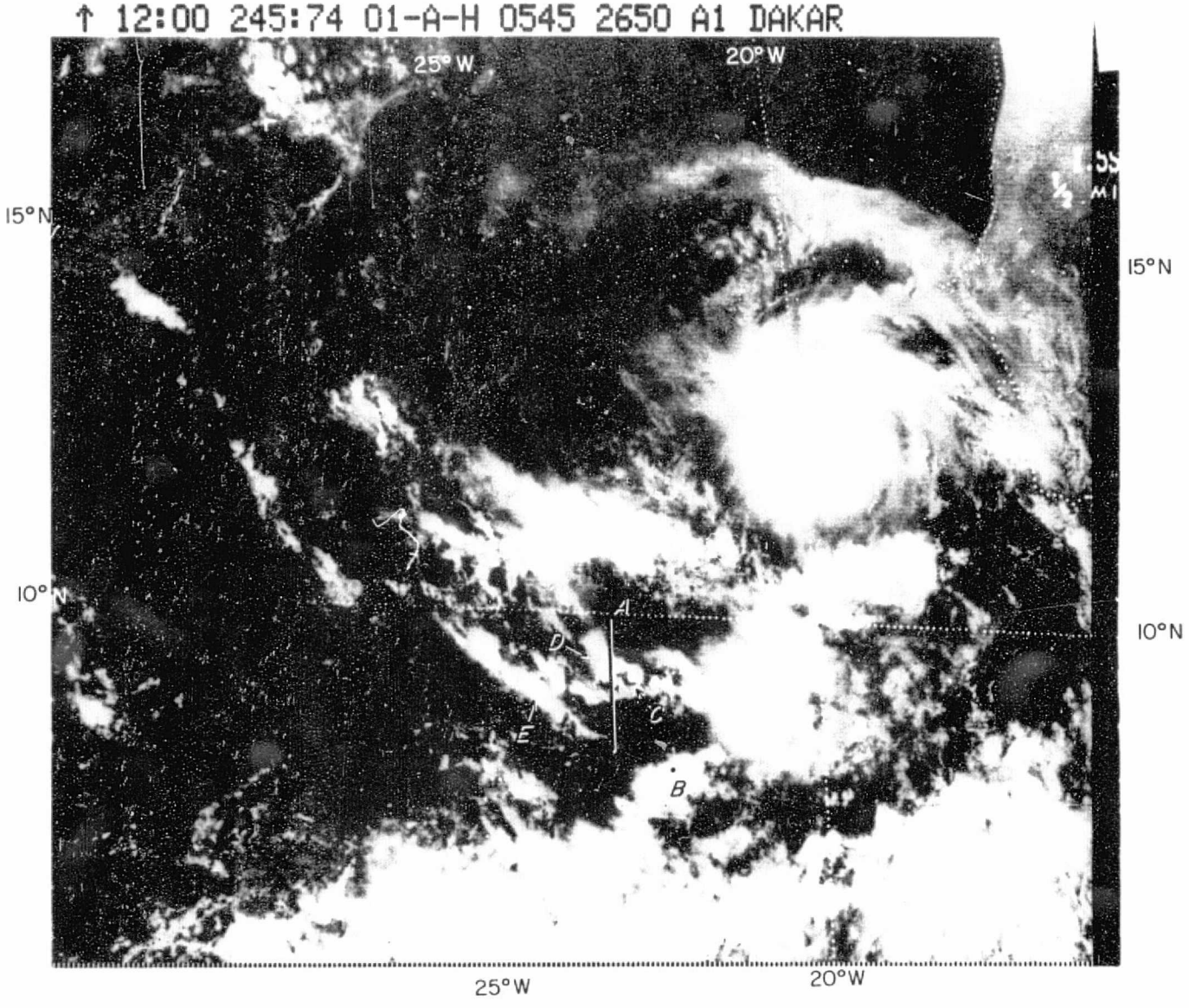

Figure 3-5 SMS Visible Imagery (1/2 mi. resolution) for 1200 GMT, 2 September 1974

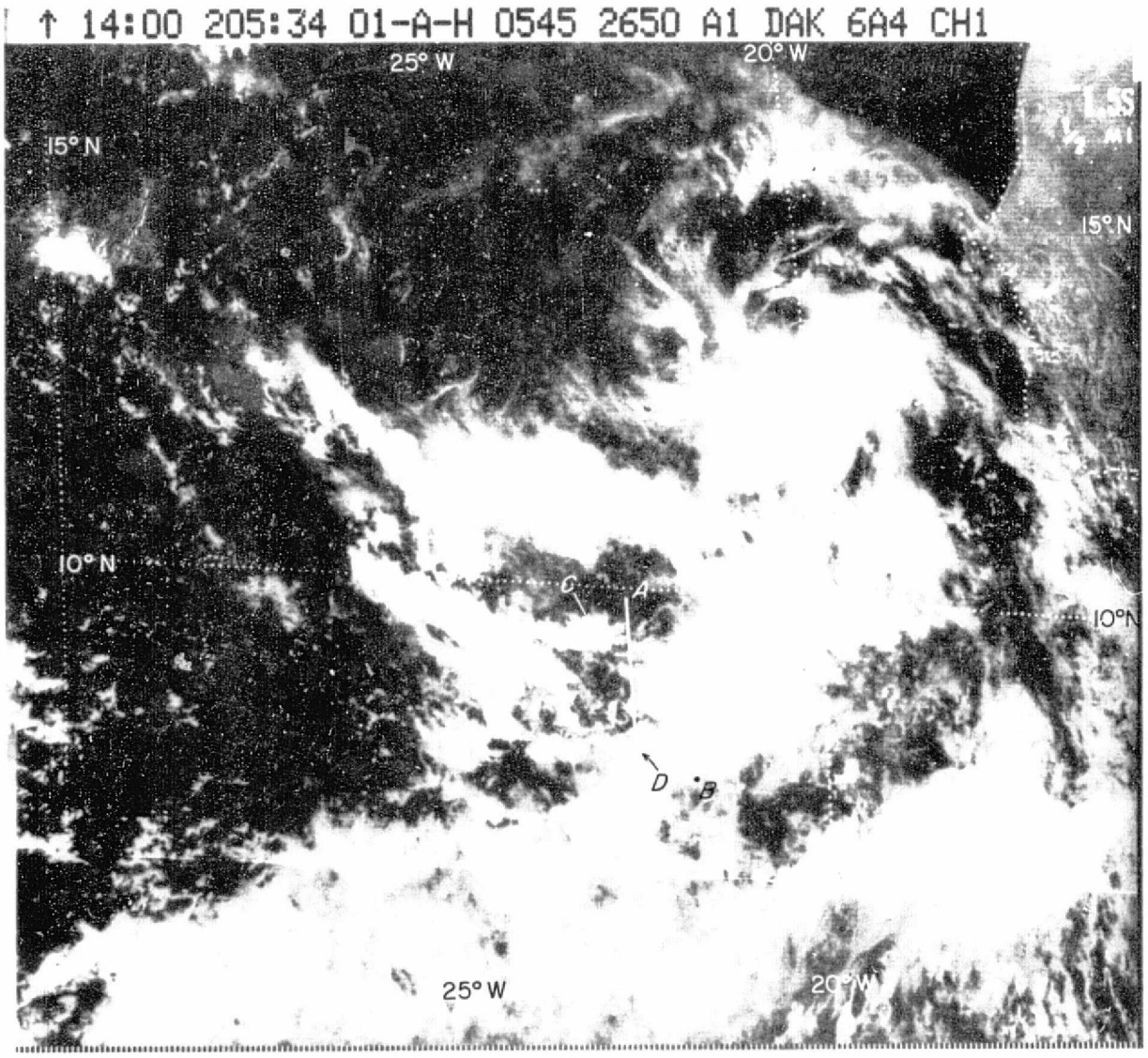

Figure 3-6 SMS Visible Imagery (1/2 mi. resolution) for 1400 GMT, 2 September 1974

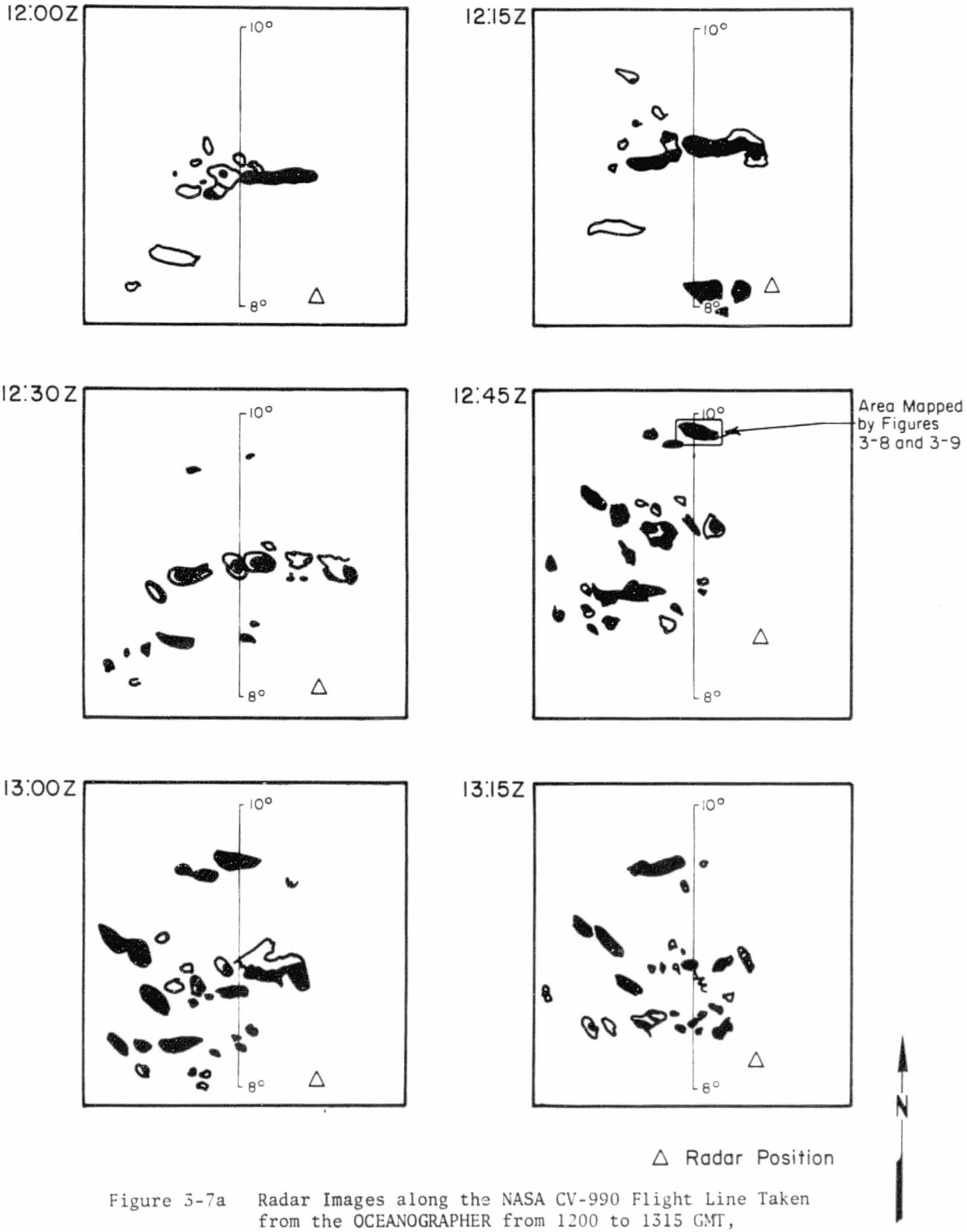

Figure 3-7a Radar Images along the NASA CV-990 Flight Line Taken from the OCEANOGRAPHER from 1200 to 1315 GMT, 2 September 1974

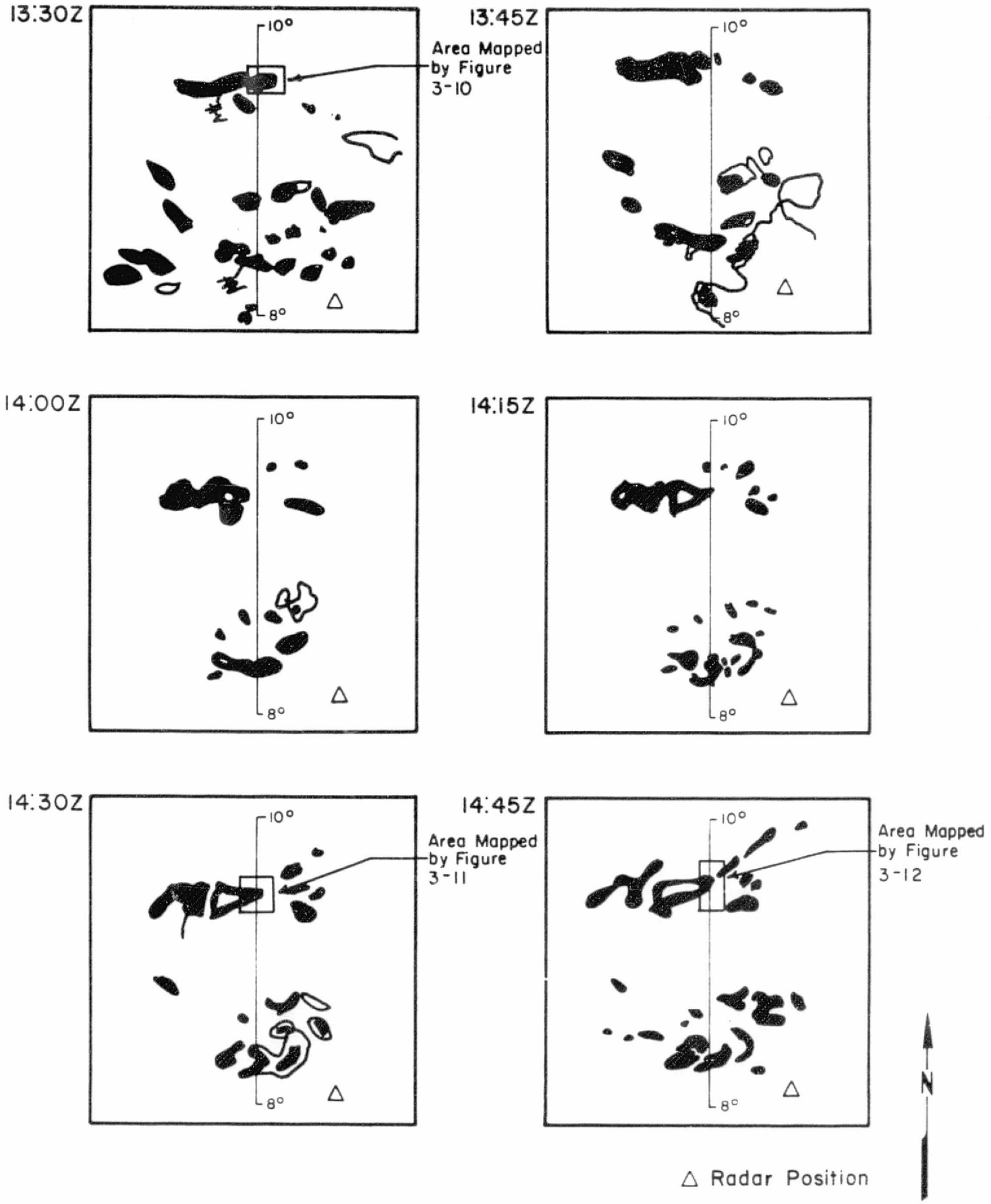

Figure 3-7b Radar Images along the NASA CV-990 Flight Line Taken from the OCEANOGRAPHER fr.m 1330 to 1445 GMT, 2 September 1974

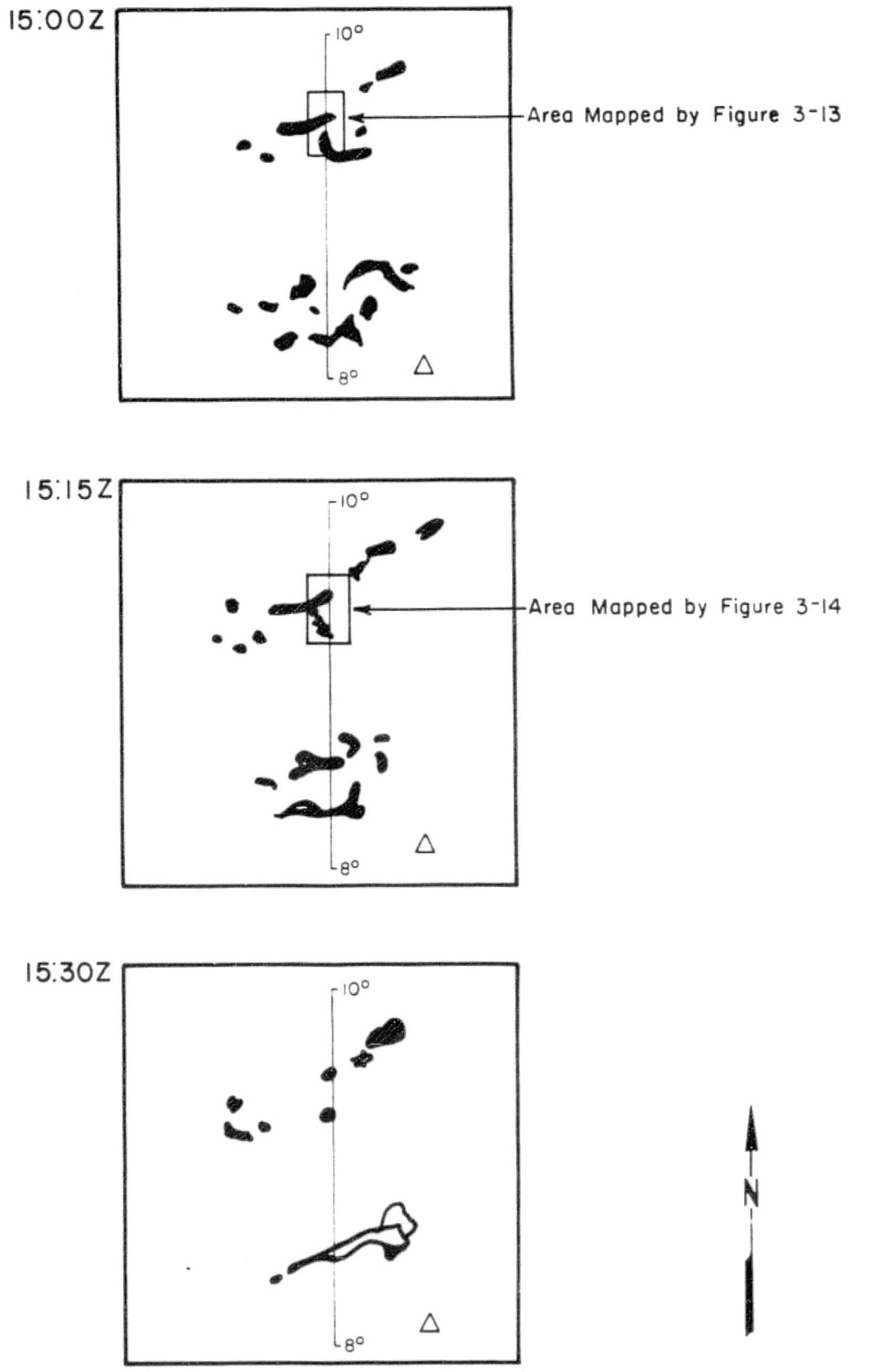

Figure 3-7c Radar Images along the NASA CV-990 Flight Line Taken from the OCEANOGRAPHER from 1500 to 1530 GMT, 2 September 1974

found in the western end of the line. Another rain area is also seen further south corresponding to the eastern tip of the wide cloud band oriented northwest-southeast west of the experiment path (point E, Figure 3-5). No rain whatsoever appears in the cloud mass located north of the east-west cumulus line.

Following the time sequence of the radar images, it becomes evident that the situation changes rapidly. The east-west cumulus line intensifies slightly, then breaks up to become a region of scattered clouds and cloud masses by 1300 GMT. A number of precipitating areas appear in the southwest corner of the images, indicating increased activity in the northeast-southwest cloud band and a spreading of that band towards the western terminus of the east-west line. Rain also appears at the northern end of the flight path with a large area of precipitation visible at 1320 GMT.

By the time of the satellite image at 1400 GMT, the clustered rain pattern had reformed into two precipitation zones. One located at the northern end of the flight path corresponds to the cloud mass visible to the west of the path (Figure 3-6, point C). The other at the southern end of the flight line appears to be part of a new cumulus line partially covered by the cirrus canopy spreading from the east (Figure 3-6 point D). Little activity is seen between these two zones with the west portion of the initial area of convective cloudiness now almost cloud-free. This pattern continued for the remainder of the mission with decay of all activity along the path finally settling in around 1500 GMT.

3.2 Microwave Measurements of a Twin-Celled Cloud Mass

Microwave measurements along the flight path were made during a series of ten passes summarized in Table 3-1. The flight paths were generally north-south or vice versa at about 20-minute intervals, and useful data were collected for about 10 km on each side of the flight path. Each pass generated a series of horizontal scans with data points separated by approximately 500 m along the flight path. In the horizontal, the width of the footprint increased from about 400 m at nadir to about 1100m at the maximum scan angle of 49°, necessitating rectification of the brightness temperature maps before cell analysis could be performed. This was accomplished by replotting the data at locations corresponding

TABLE 3-1

NASA CV-990 MEASUREMENT RUNS

MISSION 245-1, 2 SEPTEMBER 1974

Run	Time						Heading (deg)	Start		Stop		Alt	
	Start			Stop				Lat N deg min	Long W deg min	Lat N deg min	Long W deg min	Start (feet meters)	Stop (feet meters)
	HH	MM	SS	HH	MM	SS							
1	12	11	46	12	23	50	179	9 40.7	22 50.0	8 06.9	22 49.9	30886.2 9414.1	30999.7 9448.7
2	12	29	22	12	37	54	360	8 30.6	22 50.0	9 40.5	22 50.3	30985.4 9444.3	30915.5 9423.0
3	12	47	05	12	56	09	180	9 41.0	22 49.5	8 31.9	22 49.7	36713.2 11190.2	36886.5 11243.0
4	13	06	40	13	15	12	2	8 33.9	22 50.2	9.41.1	22 50.2	36948.2 11261.8	36646.1 11169.7
5	13	21	03	13	35	06	179	9 43.1	22 50.2	8 10.0	22 49.5	24980.1 7613.9	24878.2 7582.9
6	13	40	27	13	55	42	360	8 13.4	22 49.7	9 53.4	22 49.8	24887.3 7585.6	24869.9 7580.3
7	14	06	55	14	23	00	180	10 07.9	22 49.9	8 04.9	22 49.8	30795.2 9386.3	30881.3 9412.6
8	14	29	20	14	43	15	360	8 05.6	22 50.2	9 56.3	22 49.8	30871.2 9409.5	30904.5 9419.7
9	14	52	05	15	05	08	177	9 55.4	22 50.2	8 12.1	22 49.9	36885.9 11242.8	36803.2 11217.6
10	15	11	20	15	24	22	1	8 12.1	22 50.2	9 57.3	22 49.3	36848.1 11231.3	36864.6 11236.3

to the center of each scan point cross track and the aircraft's position downtrack. Despite some remaining distortion, this procedure generated reliable precipitation maps in good agreement with the radar images. Contouring of the data used the brightness temperature levels shown in Table 3-2 to provide rain rate increments of 3 to 4 mm hr^{-1}. As indicated in Section 2, these rain rates should not be interpreted as absolute values but rather numbers accurate to approximately 2 mm hr^{-1}.

Figures 3-8, 3-9 and 3-10 show the precipitation structure of the cloud mass first visible on the radar at 1230 GMT (see Figure 3-7). These radiometric maps were taken at 1237, 1247, and 1322 GMT, respectively, and cover the period from the onset of rain through the mature stage. Since the rain band was near the north end of the flight path, data intervals on the rain varied from 10 to 30 minutes. Subsequent maps showed the dissolution of this system but are of little interest except in identifying that the length of the mature cloud stage was two hours.

The primary feature of this cloud mass is the twin-celled pattern characteristic of the three figures. These cells represent two separate cumulus congestus which developed in unison, became cumulonimbi together and eventually disappeared into a broad, diffuse area of light rain. To the radar, they appeared as one very large storm with no cellular structure discernible, an appearance probably due to the fact that they acted in tandem and formed one continuous rain pattern.

When this region was first observed at 1212 GMT, it was characterized solely by small nonprecipitating cumulus and altocumulus with a cirro-stratus layer far above. From these clouds, in the period of only twenty-five minutes, emerged the two large cumulus congestus seen precipitating in Figure 3-8. In an early mature stage, these clouds were not glaciated and their rain rate patterns appeared quite uniform and sharply defined. Both cells were considerably elongated, with cores of 10 mm hr^{-1} rainfall approximately 4 km long and 1 km wide and overall rain patterns covering regions of 9 km by 4 km. The clouds were so close that no clear area could be observed between them; in fact, there were indications that new development was being spawned between them.

During the next ten minutes, the tops of the clouds were observed to be glaciating, a process possibly encouraged by seeding from the cirrostratus layer above. Remarkable intensification has occurred in

TABLE 3-2

MICROWAVE GREY SCALE CATEGORIES

Level	Minimum Brightness Temperature	Minimum Rain Rate (from Wilheit et al, 1975)
1	175°K	0.8 mm hr^{-1}
2	200°K	3 mm hr^{-1}
3	225°K	7 mm hr^{-1}
4	240°K	10 mm hr^{-1}
5	250°K	14 mm hr^{-1}
6	260°K	20 mm hr^{-1}

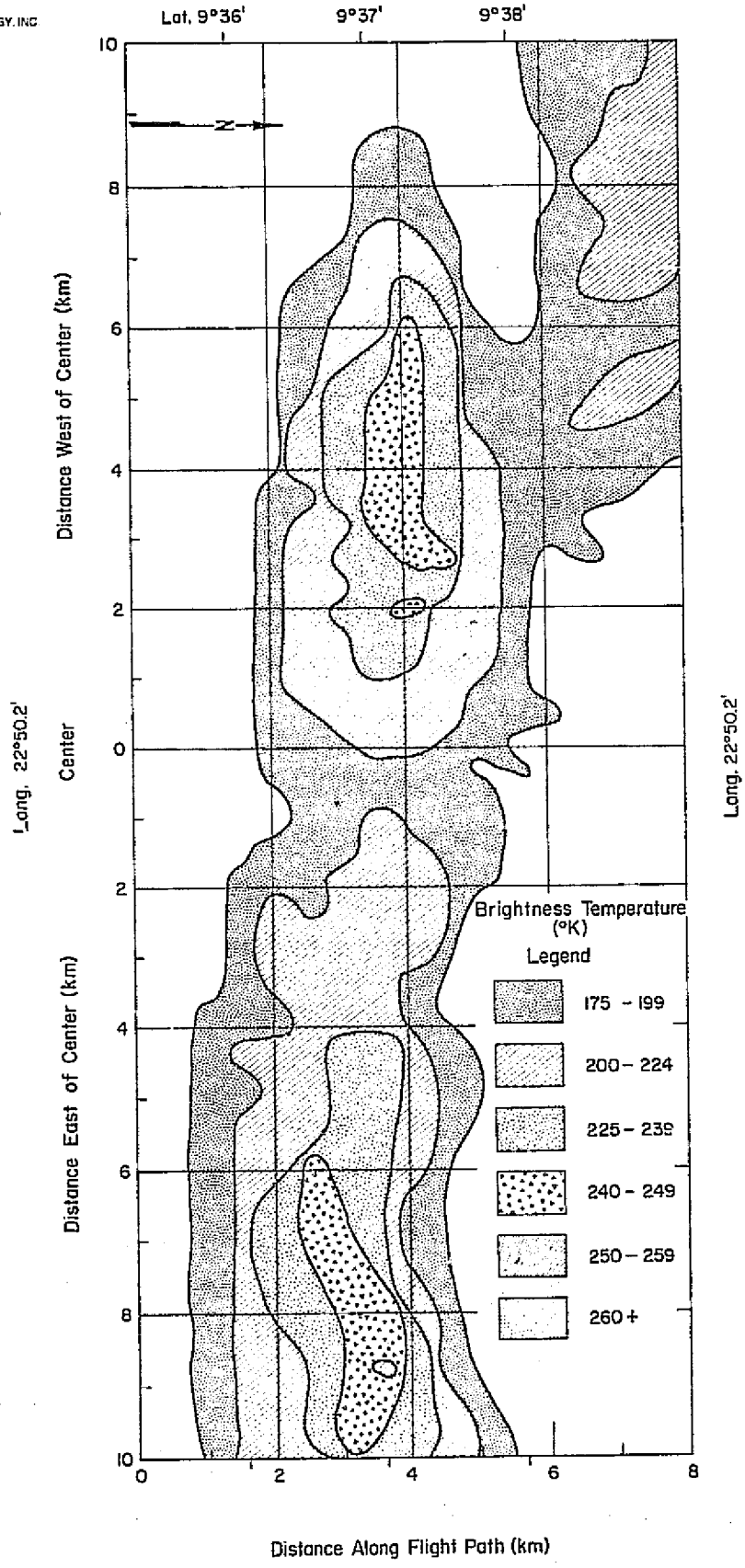

Figure 3-8 Microwave Imagery of the Twin-Celled Cloud Mass at 1237 GMT, 2 September 1974

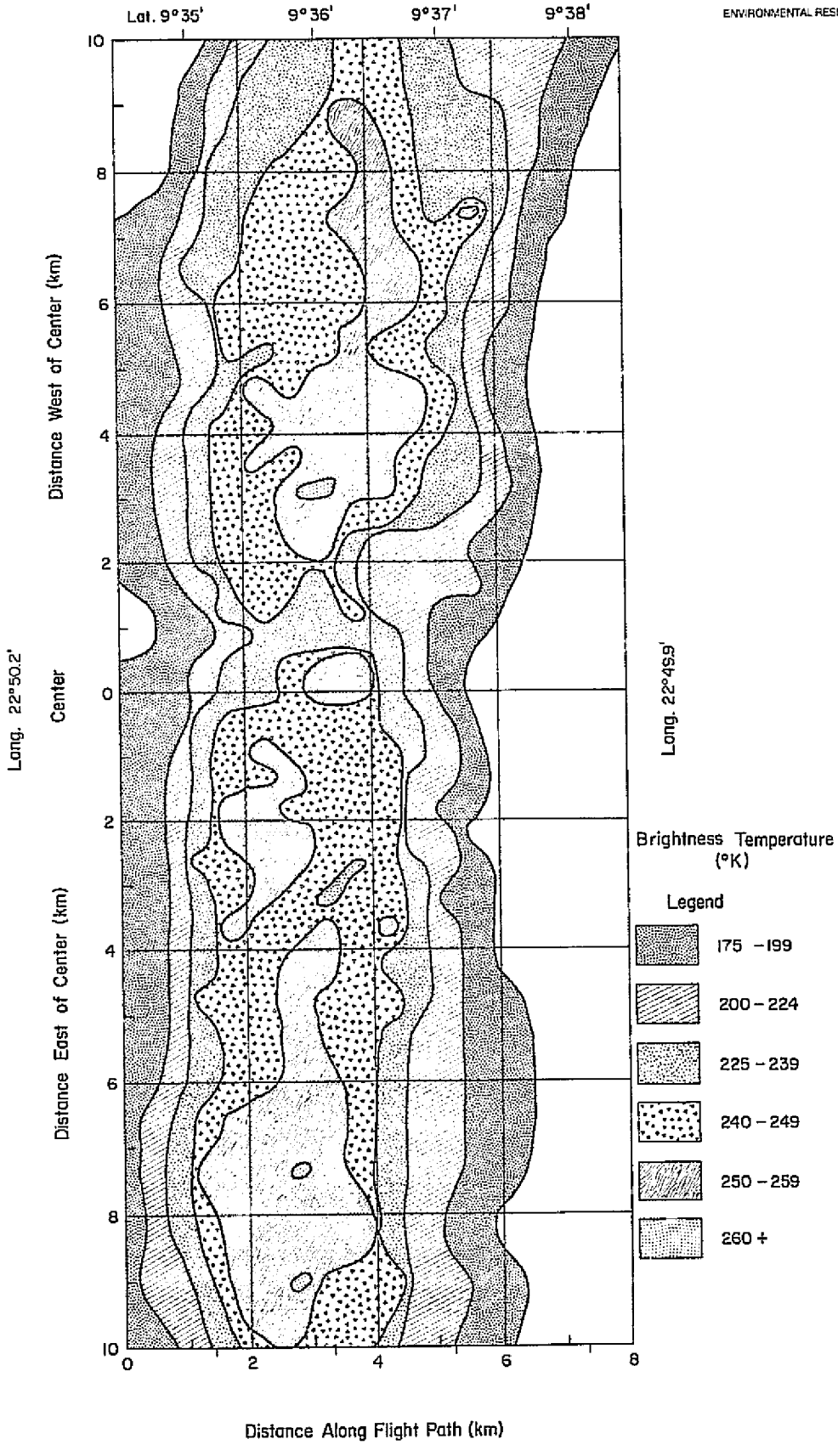

Figure 3-9 Microwave Imagery of the Twin-Celled Cloud Mass at 1247 GMT, 2 September 1974

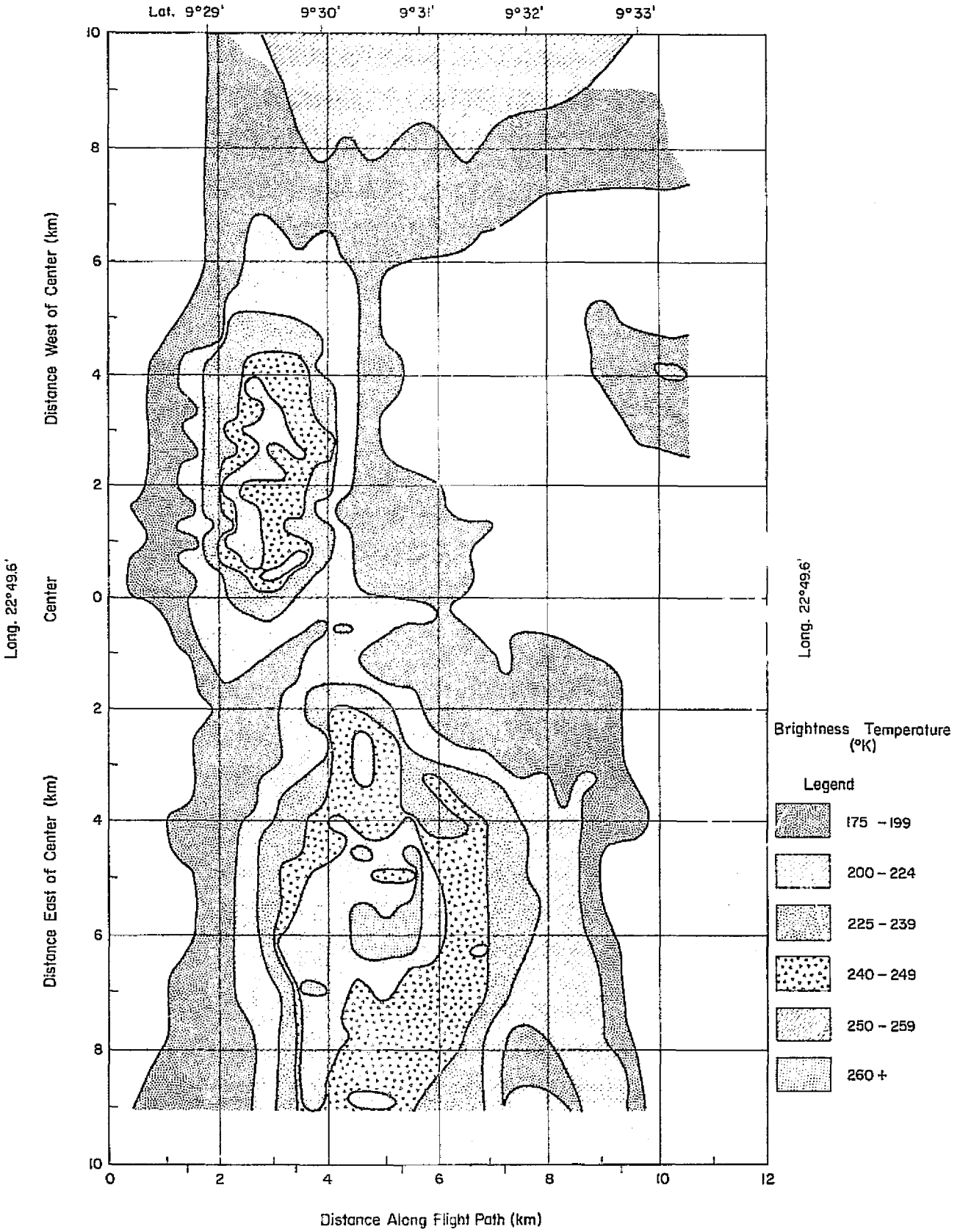

Figure 3-10 Microwave Imagery of the Twin-Celled Cloud Mass at 1322 GMT, 2 September 1974

the size and intensity of the rainfall area (see Figure 3-9), while the radar data showed ice particles up to altitudes of 8 km and rain from 4.5 km, just below the melting level. On the ESMR maps, the two cells showed rain rates greater than 14 mm hr^{-1} over areas 6 km long by 4 km wide with pockets of even higher readings (e.g., 20 mm hr^{-1}) and uneven contours characteristic of mature cumulonimbi. This core intensification was also reflected in the growth of the entire rain area to cover a region more than 20 km long and 7 km wide.

Of particular interest is the appearance of two very intense cumulus congestus clouds between the two large cumulonimbi. These cells have emerged from the western portion of the eastern cell to go from rain rates less than 7 mm hr^{-1} to values greater than 14 mm hr^{-1} in the 10-minute time span. Such growth reflects the considerable convective activity which would be expected in the zone between two well-developed convective clouds due to the interaction of the wind fields. In fact, early thunderstorm research (Byers and Braham, 1949) defined this zone as the most likely region for the development of new cells. Both of the new cells have caused some deformation of the original rain patterns, indicating that they themselves have developed well-defined flow fields. Such deformation also occurs on the northeast flank of the western cell, hinting of a new cell there.

The subsequent aircraft pass over the area was on a track slightly west so it showed merely that the western cell still had rain rates exceeding 14 mm hr^{-1} and was continuing its southward movement. The cloud mass was reencountered, however, during the following pass at a time thirty-five minutes later than that of the measurements discussed above. Figure 3-10, taken at this time, shows that the original cells are still clearly discernible, with rain rates in the cores still of great intensity, but that several changes have occurred. For one, the western cell is now significantly decreased in size and is positioned slightly to the south of the eastern cell. This may be partially due to the effects of a small cell on the northeast flank but is probably also a result of its smaller relative size. In either case, it marks the loss of a consistent flow field throughout the cloud mass and the beginning of its dissolution. Reference to the radar images reveals that the system is

now coming under the influence of a larger cloud mass to the west, making it probable that the changes seen here are due to the cloud mass interactions.

In contrast to the western cell, the eastern cell has continued unabated in size or intensity, although its internal structure has changed slightly. Both the small central intense cell and the tiny weak cell which appeared in Figure 3-9 are still visible but the larger cumulus congestus cannot be found, nor can the original cumulonimbus core be readily identified. High-resolution radar studies (e.g., Barge and Bergwall, 1976) have shown that precipitation zones on the order of 1 km in diameter frequently have lifetimes in the tens of minutes and that such cells develop and dissipate in the same portion of a larger storm system. This is evident here in the convective zone occurring along the boundary of the two large cumulonimbi.

Later passes over this area showed that the clouds steadily dissipated from this time on. The entire system ceased to move south, and began to move west to meet the larger cloud mass. It also proceeded to disappear into a broad area of light rain with almost no identifiable structure, behavior that would be expected of decaying storms with strong downdrafts. The final traces of precipitation disappeared approximately two hours after they were first detected and it seems likely that the storms did not survive to merge with the other cloud mass.

Several features of this cloud mass are quite interesting. For one, there is no evidence of cell merger between the two cumulonimbus clouds; in fact, their final separation verifies that they have retained their individual identities throughout all phases of development, maturity, and dissipation. In fact, the behavior of the system is quite similar to that observed in midlatitude storm lines (see, for example, Warner, 1976) characterized by large intense precipitating cells with diameters on the order of 10 km and lifetimes on the order of 100 minutes, and by smaller shorter-lived cells between the main cells. The large-scale flow field and system movement also reflects that observed in squall lines and indicates that this tropical cloud mass has similar properties to that of organized convective activity often found in higher latitudes.

Another feature of interest is the parallel life cycles of the two cumulonimbi. In most cases of multicloud systems, one cell develops, then another, and so forth, with differing start and end times for the individual clouds. In fact, the prior existence and dissipation of some clouds appears to favor the subsequent development of other clouds. This was not apparent here, since both visual and microwave observations showed tandem behavior with the two cells either independently thriving on the same convective conditions or, more probably, interacting to the mutual benefit of both. The slightly earlier dissipation of the western cell when influenced by another cloud mass also suggests that the uniform flow field around the twin cells was to their advantage and that cloud interaction at later stages of development might be detrimental. This point will be explored further below.

3.3 Microwave Measurements of Cloud Mass Mergers

One frequently observed phenomenon during GATE was the tendency of different clouds to move in different directions in the same region. This was partly due to the variety of altitudes from which the cells developed and to the variety of cloud sizes, but it applied as much to organized clouds as to isolated clouds. Occasionally lines of clouds even crossed one other and continued on unchanged (Geotis, 1975), but more often clouds merged to form larger masses or to dissipate. Such an event occurred during Mission 245-1 to form the three-pronged cloud mass seen in the radar imagery of 1515 GMT (Figure 3-7).

Observations of the region just south of the twin-celled cloud mass showed a series of large, connected cells building to the west as the older clouds to the north glaciated. These clouds have been mentioned above as the western cloud mass whose development coincided with the decay of the twin-celled system. After the disappearance of the twin-cells, the tip of this cloud mass moved east under the flight line and remained there for the duration of the experiment. Eventually, another large cloud moved in from the northeast to join the western mass. Its arrival was soon followed by that of a long cloud line coming from the southeast. Since these mergers all occurred under the flight path, it was possible to obtain information about the effects of cloud mass convergence.

Figures 3-11 through 3-14 show the microwave precipitation patterns found along the flight path in the region between 9°08'N and 9°25'N at times of 1422, 1439, 1456 and 1520 GMT, respectively. The tip of the western cloud mass is seen between latitudes of 9°18'N and 9°25'N in all four figures, where it covers the western portion of the swath. When initially sampled (Figure 3-11), a small cell was seen at its leading edge followed by a much larger, well-developed cloud mass and preceded by an isolated area of very weak rain.

The precipitation pattern and horizontal structure of this cloud mass changed with time in contrast to the twin-celled cloud mass described previously. At 1422 GMT the cloud was developing and was characterized by a main rain core of rain rates between 10 and 14 mm hr^{-1}. However, this core was highly irregular in shape, indicating that the mass was composed of several convective elements rather than identifiable large clouds. This indication was confirmed by examination of the data taken 17 minutes later and shown in Figure 3-12; in this figure an entirely different structure is evident and is dominated by two large rain cores and several small cells. The system as a whole had greatly intensified in rain rate (now greater than 20 mm hr^{-1}), in width, and in vertical extent (precipitation to 3.5 km, ice to 10 km) and was associated with noticeable aircraft turbulence at an altitude of 9.7 km.

Such development, in conjunction with the varying precipitation patterns and the lack of system motion, identifies a region of cells undergoing continual growth and dissipation with newer cells possibly feeding upon the moisture fields left by the old. In fact, it is difficult to determine whether this is one multicelled storm or a group of identifiable cloud systems.

Twenty minutes later, observations again showed different precipitation patterns but the convective activity characteristic of a mature cloud was still present (Figure 3-13, note scales reduced). Rain rate intensity still exceeded 14 mm hr^{-1} for most of the region and radar indicated that the rain extended between the melting level of 5 km and the surface. Both visual and radar observations showed that the mass had glaciated with the cirrus layer extending to the aircraft altitude of 11.7 km. This mass now appeared as a single massive, mature cumulonimbus.

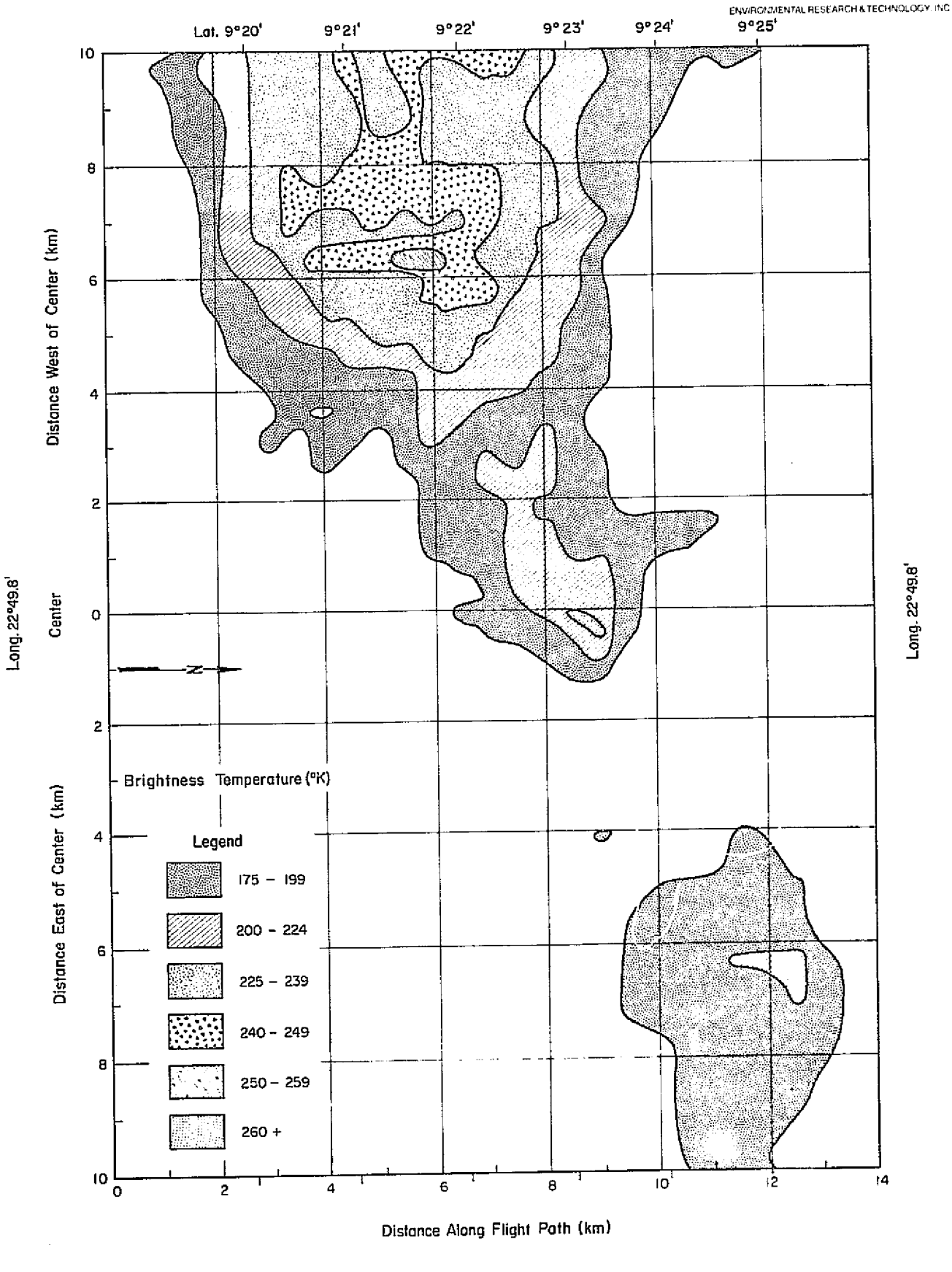

Figure 3-11 Microwave Imagery of the Tip of a Cloud Mass at 1422 GMT, 2 September 1974

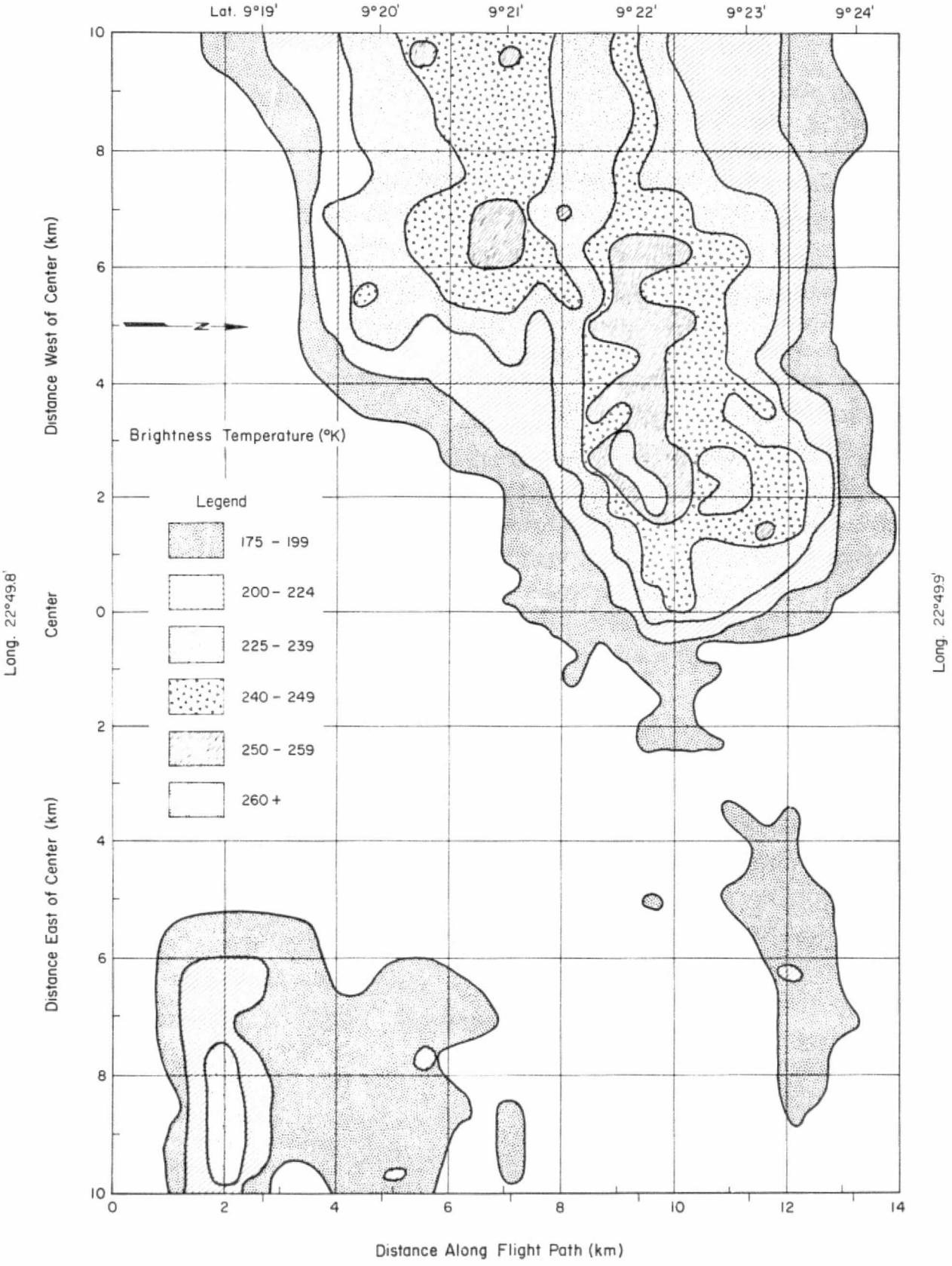

Figure 3-12 Microwave Imagery of the Tip of a Cloud Mass at 1439 GMT, 2 September 1974

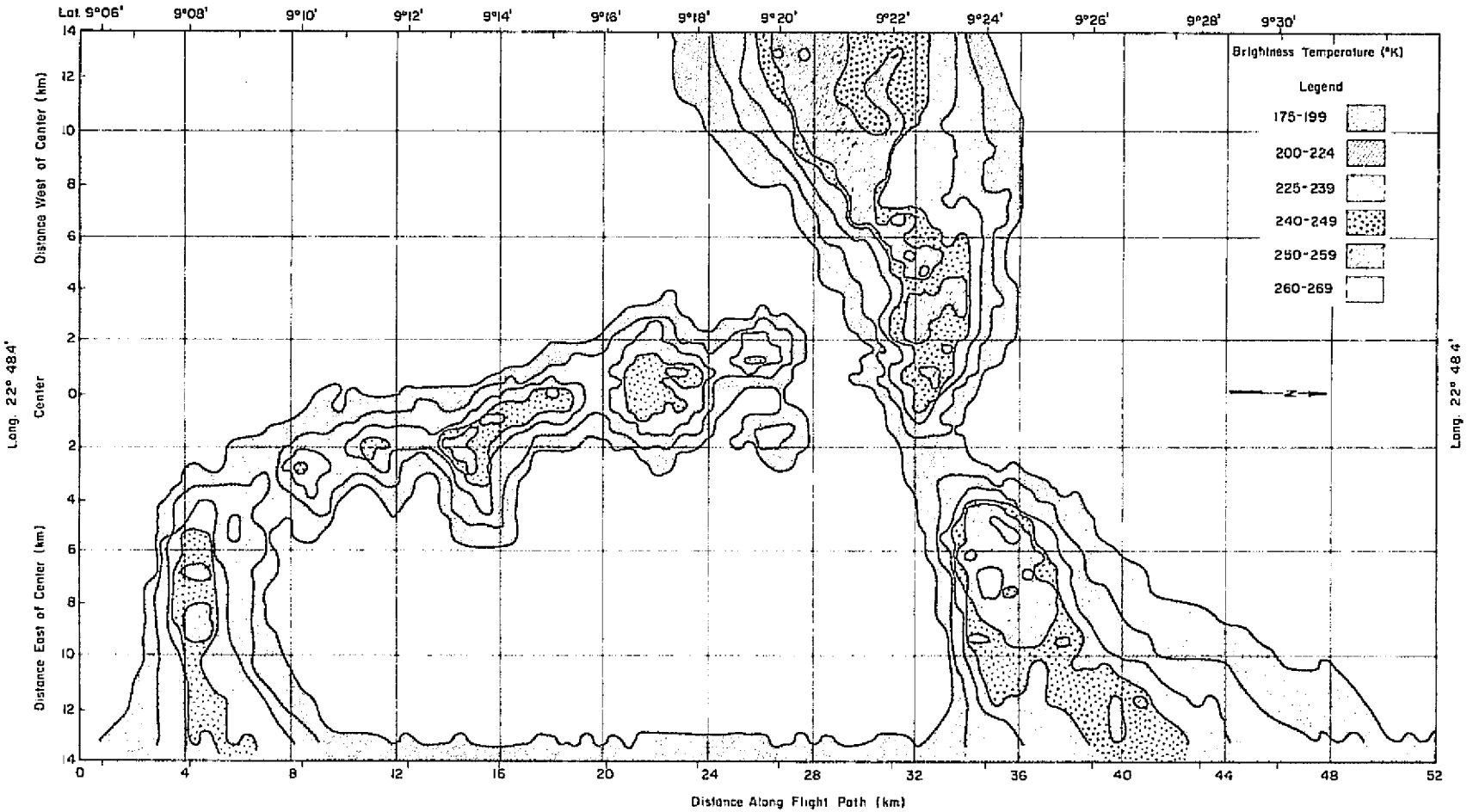

Figure 3-13 Microwave Imagery of the Tip of a Cloud Mass, a Cloud Line and a Cumulus Congestus at 1456 GMT, 2 September 1974

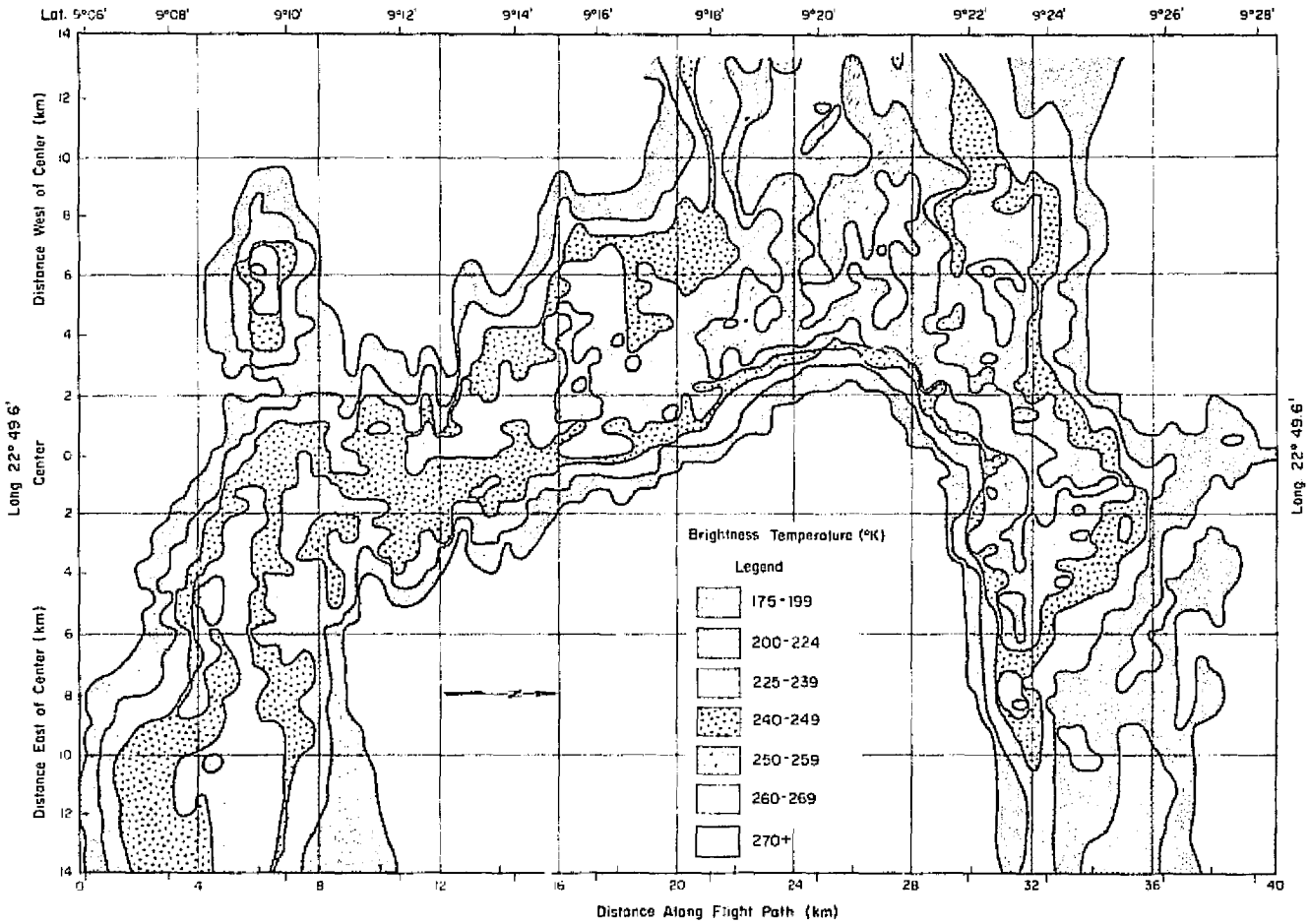

Figure 3-14 Microwave Imagery of the Combined Cloud Mass, Cloud Line and Cumulus Congestus at 1520 GMT, 2 September 1974

In contrast to the maturity and gradual decay of this cloud mass, the rest of the region showed remarkable development after 1439. A large cumulus congestus had appeared northeast of the cloud mass with rain rates exceeding 20 mm hr^{-1} and a rain area which overlapped that of the cumulonimbus. A long, curved line of small rain cells also had developed southeast of the mass with rain rates frequently exceeding 10 mm hr^{-1}. This band was separated from the cloud mass by 1 km and visual observations showed it to be growing rapidly.

Reference to the radar imagery of Figure 3-7 shows that shortly after this pass the northeast cumulus congestus joined the cloud mass. By 1510 GMT, a fairly solid line had also formed. The result of these mergers was the massive, multicellular rain pattern seen in Figure 3-14. This rain pattern differs substantially from those previously seen, in that clearly defined cell structure has been replaced by long, interconnected rain bands of variable width and spacing. The northeast cloud, which merged earlier, has undergone extensive dissipation and the merged zone has developed a completely new precipitation structure characteristic of neither the cumulus congestus nor the cloud mass. Such changes are also evident at the newer boundary formed by the cloud line and cloud mass. There, some of the original cell structure is still evident, though distorted, but a region of very high rain rates has developed. The southern end of the cloud line has also intensified, causing severe turbulence at 11.7 km. In the radar imagery (Figure 3-15), the entire region (9°08'N to 9°27'N) shows surface rain rates of 7 to 30 mm hr^{-1} and precipitation to altitudes of 8 km, well above the melting level, confirming the microwave- and aircraft-deduced conditions of strong vertical velocities.

The implications of this precipitation pattern are several. Although the time difference between passes was too great to allow study of individual cell histories, it is clear that the clouds did merge and lose their identities. Although the individual cells could not be followed with certainty from succeeding maps, it seems that the merger caused the disappearance or destruction of old cells and favored the development of new convective activity at the boundaries of the merged clouds. This new convective activity was extremely intense and occurred generally along a thin line rather than in identifiable cells; it was

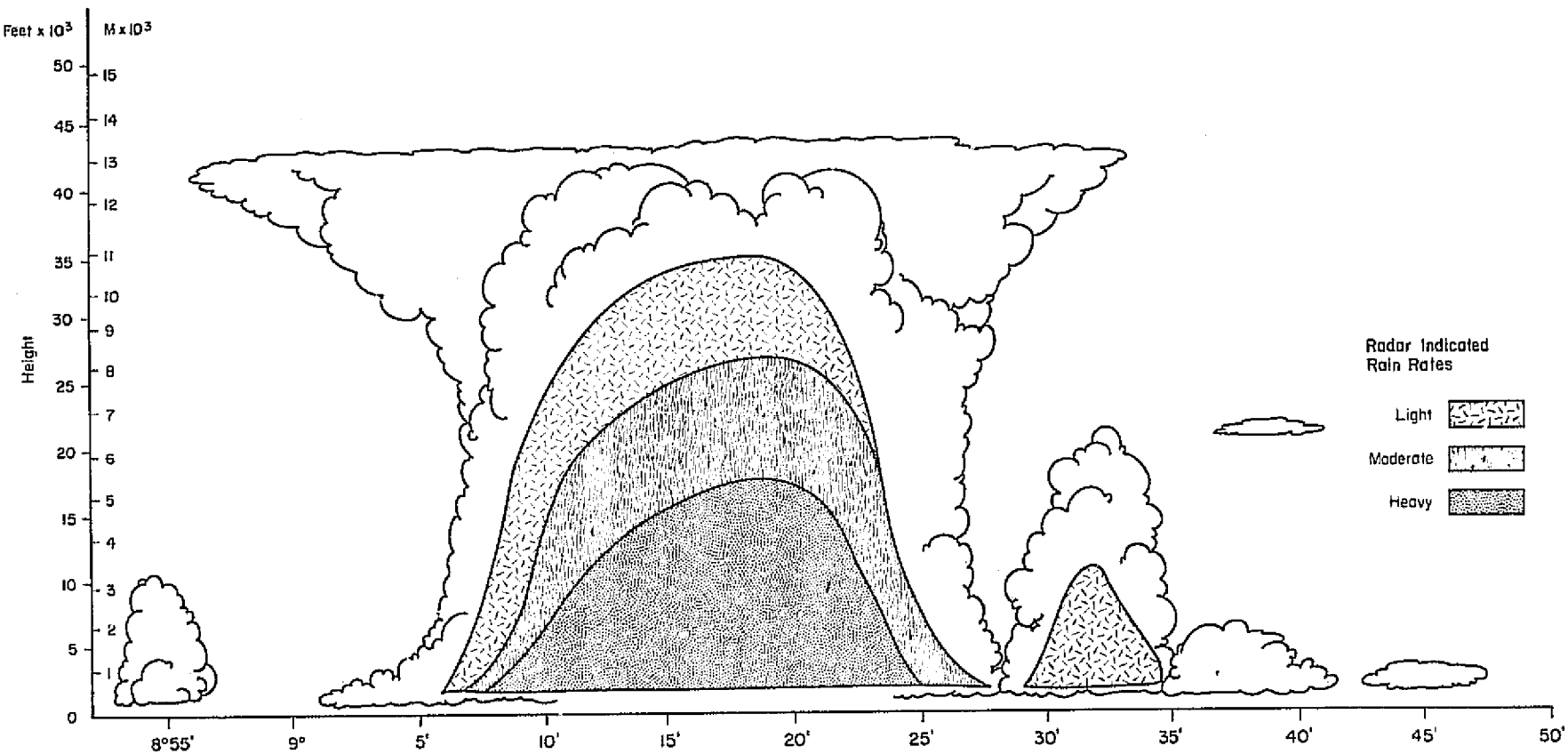

Figure 3-15 Radar Imagery of the Combined Cloud Mass, Cloud Line and Cumulus Congestus System

however, very short-lived. Only small areas of precipitation were evident fifteen minutes later in the radar images (Figure 3-7 1530 GMT). Radar imagery given by Woodley and Simpson (1972) showed the same marked change in precipitation patterns when clouds merged, but their data showed high rain rates for long time periods. However, since their measurements were at a much lower spatial resolution, it is not clear that their observations represented the same type of cloud merger seen here. Indeed, on the basis of the two cases analyzed in this section, it may be that the maximum precipitation amounts occur from cloud masses which are formed from individual clouds with similar life cycles but unique identities, and that the merger of well-developed cells leads not to steady-state systems but rather to explosive growth and decay.

4. THE EFFECTS OF PRECIPITATION ON SATELLITE MICROWAVE MEASUREMENTS

The discussions of the two previous sections have concentrated upon the inference of rain rates from aircraft microwave data. However, they have clearly identified many features of importance to the inference of rain rates from satellite microwave data. The aircraft measurements have shown that the theoretically derived microwave-rain rate relationships are valid to within 2 mm hr^{-1} and that radiometric data obtained at heights of 7 to 12 km can be inverted to provide reasonable estimates of surface rainfall rates. The derived relationships should be applicable to satellite measurements, provided that the precipitation covers large areas, since the radiometric values were collected above the precipitation layers and little difference in brightness temperature would be expected from atmospheric contributions between aircraft and satellite altitudes.

Analysis of precipitation cases measured with the aircraft ESMR, however, has pointed out a feature which would cause significant differences between aircraft and satellite measurements - the spatial resolution. For the Nimbus 5 ESMR, the optimum resolution is 25 km by 25 km, an area exceeding that of most of the cloud masses discussed above. In addition, the cloud masses sampled showed substantial rain rate changes within a few kilometers or less, with the most intense rain rates generally occupying only a small portion of the entire system. Since these high rain rate areas are significantly smaller than a satellite scan spot, it is unlikely that very high (> 240°K) brightness temperatures and corresponding high rain rates will be sensed from space. This, then, leads to a question of the applicability of the relationship derived in Section 2 to the determination of rainfall from satellite data.

To investigate this problem, Nimbus 5 ESMR collected over the GATE area on 2 September 1974 was analyzed and compared with the radar data from the OCEANOGRAPHER. Figures 4-1 and 4-2 show the microwave and radar data sets collected near 1300 GMT in the region between 7° and 10°N and 20° to 25°W. In this case, the satellite data was left unrectified with the radar data replotted to be at the same scale. Thus, the east-west dimension is squeezed compared to the north-south dimension.

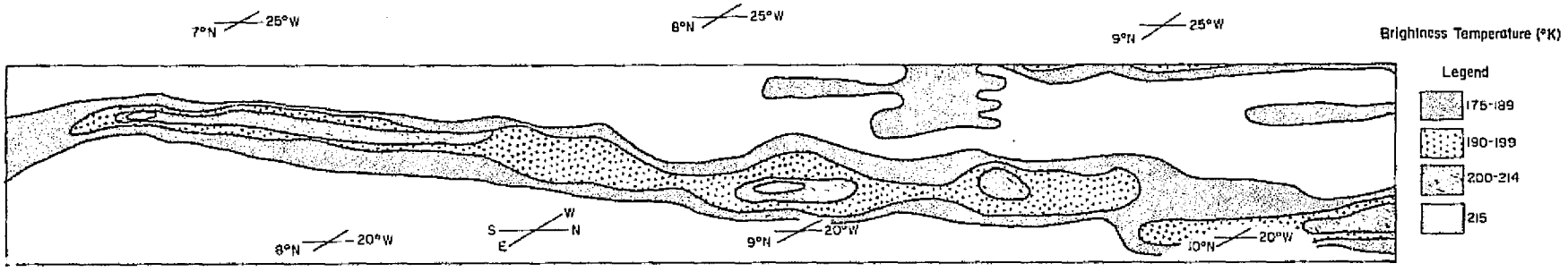

Figure 4-1 Nimbus 5 Microwave Imagery of the GATE area at 1300 GMT, 2 September 1974

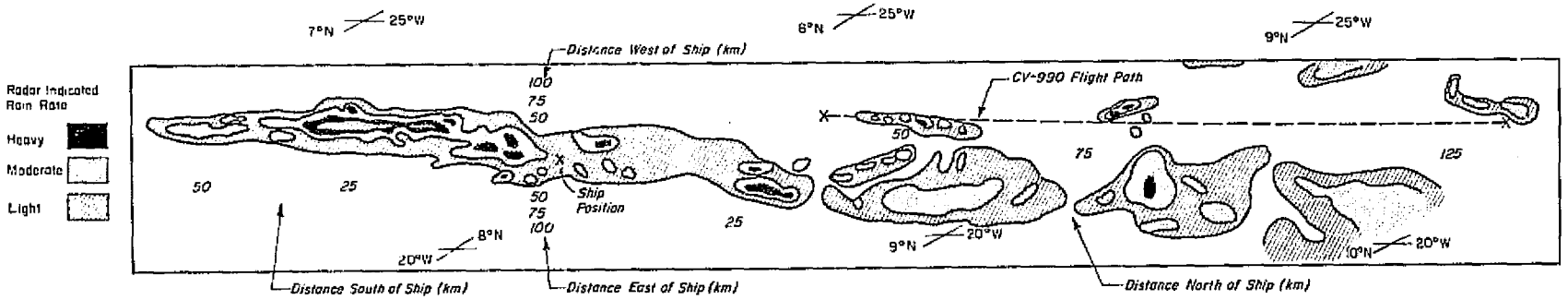

Figure 4-2 Radar Imagery of the GATE area at 1300 GMT, 2 September 1974

The line indicated by the X's on Figure 4-2 marks the flight path, with the cloud mass at the northern tip being the twin-celled system. Most of the rain areas seen here belong to the main cloud system indicated in Figures 3-5 and 3-6 by the large cirrus shield east of the flight path. This system is characterized by an elongated rain band 50 to 75 km wide and at least 175 km long, although rain is not continuous throughout the region (Figure 4-2). In fact, the first grey level shown in the radar imagery is indicative of light scattered rain of an intensity which often cannot be seen on the scale used here.

It is readily apparent that the high brightness temperatures seen in the aircraft data do not occur in the data observed by satellite (Figure 4-1). The maximum values seen are 215°K, corresponding to rain rates near 3 mm hr^{-1} (see Figure 2-1). In fact, all of the brightness temperatures indicate rain rates on the low end of those shown by the radar (Figure 4-2), while the aircraft microwave measurements indicated rain rates significantly higher than those shown by radar. The low satellite readings correspond to the low resolution factors, since the radar imagery reveals that few grey scale values extend a full 25 km along the orbital track (although many are 25 km wide). This is especially true for the higher reflectivity levels (e.g., the zone near 7.5°N, 23°W) which have the smallest areal extent.

If one spatially averages the radar data to obtain a rain rate corresponding to the satellite footprint, one finds good agreement between the two data sets and the derived microwave rain rate relationship. The higher brightness temperatures (> 210°K) occur in regions when rain rates from 1.8 to 7 mm hr^{-1} are shown for areas at least 250 km^2. Brightness temperatures from 205 to 210°K are found in surrounding areas where rain rates from 2.0 to 7 mm hr^{-1} are indicated, with values greater than 1.8 mm hr^{-1} dominating. Finally, brightness temperatures from 175°K to 200°K represent locales characterized by extensive light or variable rain. In all cases, the satellite measurements can be inferred to give areal rain rates within the spatially averaged grey scale levels. In fact, the values agree within a few mm hr^{-1}; this is excellent agreement considering the poor resolution of the radar grey scale categories (see Section 2).

As a check on the findings indicated above, approximate areal-weighted brightness temperature was computed for the twin-celled cloud mass shown in Figure 3-9. Assuming that the system was located completely within the field of view, that no rain occurred in the surrounding area, and that the midpoint of each analyzed range would be used, a brightness temperature near 170°K was derived. This is in reasonable agreement with the satellite measurement of 177°K, although neither value would permit the deduction of the intense precipitation cores found in the cloud mass. Rather, the data indicates a broad area of very light diffuse rain, more stratiform than convective in character.

The effects of the large areal averaging inherent in satellite radiometric measurements do much to explain the contradictory findings of Sabatini et al (1975) and Wilheit et al (1975). If attempts are made to correlate satellite measurements with rain rate ground truth without the spatial averaging needed for a footprint, the derived microwave-rain rate relationships will show much lower brightness temperatures for each rain rate than those derived from theory. Likewise, spatially averaged rain rates will generally run considerably lower than point source measurements, leading to a bias in the brightness temperature measurements towards lower values. The result of these effects led Sabatini et al (1975) to derive an empirical microwave rain rate relationship with maximum values of 220°K. Both satellite measurements made during GATE of cyclonic systems (not shown) and previous measurements made of hurricanes (Allison et al, 1974) show that the limit on 220°K is exceeded when heavy rainfall occurs over a large area; furthermore, the aircraft measurements described in the study demonstrate that the theoretical limits of 260 to 270°K are quite valid. In fact, analysis of the spatially averaged rain rates seen here shows that satellite data are quite useful for inferring areal rain rates with the relationships presented in Section 2.

5. CONCLUSIONS AND RECOMMENDATIONS

In this study, microwave data collected during the GATE experiment from NASA CV-990 aircraft and the Nimbus 5 satellite have been analyzed to determine the effects of rain on microwave measurements and the usefulness of microwave data in studying rain. It was found that the relationship between brightness temperature and rain rate, derived from aircraft data and radar measurements, showed good agreement with the theoretically derived relationships for tropical conditions, and that the inference of rain rates from aircraft radiometric data should be possible with an accuracy of 2 mm hr^{-1}. It was also found that this relationship applied to satellite measurements if one takes into account the effect of averaging rain rate over very large areas; little information about rain rates from small areas in cells can be determined from space.

Analysis of two cloud masses, sampled during the GATE experiment with the aircraft ESMR, showed considerable cloud structure; individual clouds whose diameters ranged from 1 km to several kilometers and whose lifetimes were proportional to the diameters were clearly identified. In the two cases studied, it appeared that the simultaneous development of adjoining clouds produced the more favorable conditions for high rain rates of long duration. On the other hand, the merger of well-developed clouds led first to very intense convective activity and then to rapid dissipation of all precipitation. In neither case was cell merger found to be associated with heavy rainfall of extensive temporal and spatial extent. However, these two cases represent only a limited sample of the available data.

It is recommended that the findings of this program be examined in greater detail. Since the microwave rain rate relationship had to be based upon crude grey-scale radar measurements due to data set availability, certain assumptions of unknown validity were necessary. These could be eliminated, and the relationship more accurately defined, if the digital radar data now available were used to provide more precise rain rate values. This is particularly desirable to determine the point of inflection in the brightness temperature-rain rate curve and to permit a better understanding of the effects of the vertical rain structure on the expected brightness temperature.

Of even greater interest is the further investigation of the structure of tropical cloud masses. Several other cases were sampled using the aircraft ESMR which could not be studied here. It is recommended that these be analyzed to determine if their structure and cell interaction confirms the preliminary conclusions drawn here, or if other factors seem to be dominant. The aircraft ESMR provides unique spatial resolution for studying precipitation patterns, and used in conjunction with other measuring devices such as radar and vertical accelerometers on lower-flying aircraft, shows great promise in furthering the understanding of cumulus dynamics. This is especially true in the study of cloud merger, cloud interaction and the behavior of multicelled systems, studies of importance not only to the modeling of energy exchange but also to the systematic application of cloud seeding.

REFERENCES

Allison, L.J., E.R. Rodgers, T.T. Wilheit and R.W. Fett, 1974: Tropical cyclone rainfall as measured by the Nimbus 5 Electrically Scanning Microwave Radiometer, Bull. of the A.M.S., 55.

Barge, B. L. and F. Bergwall, 1976: Fine scale structure of convective storms associated with mail production, Second WMO Scientific Conference on Weather Modification, Boulder, Colorado.

Byers, H. R. and R. R. Braham, Jr., 1949: The thunderstorm, Washington, D.C.

Fowler, ... G., K. R. Hardy, and N. D. Sze, 1976: The development of a model to infer precipitation from microwave measurements, Final Report, Contract No. NAS5-20868, Environmental Research & Technology, Inc.

Geotis, S. G., 1975: Look ma, the twain met, 16th Radar Meteorology Conference, Houston, Texas.

Hudlow, M. D., 1975: Description and organization of radar images on 16m microfilm, unpublished manuscript, NOAA World Data Center A.

International Scientific and Management Group (ISMG), 1975: Preliminary scientific results of the GARP atlantic tropical experiment, GATE Report No. 14, WMO.

Marshall, J.S. and W.M. Palmer, 1948: The distribution of raindrops with size, J. Meteor., 5.

Rao, M. S. V., W. V. Abbott III and J. S. Theon, 1976: Satellite-derived global oceanic rainfall atlas (1973 and 1974), X-911-76-116, NASA Goddard Space Flight Center.

Sabatini, R. R., D. L. Hlavka, and R. Arcese, 1975: Applications of the Nimbus 5 ESMR to rainfall detection over the oceans and to sea-ice detection, Final Report, Contract No. N66314-73-C-1572, Earth Satellite Corporation.

Simpson, J., W. H. Woodley, and A. H. Miller, 1971: Precipitation results of two randomized pyrotechnic cumulus seeding experiments, J. of Applied Meteorology, Vol. 10.

Warner, C., 1976: Case studies of seeded Alberta hailstorms, Stormy Weather Group Scientific Report MW-86, McGill University.

Woodley, W. L. and J. Simpson, 1972: Results of dynamic multiple cloud seeding in Florida, Third Conference on Weather Modification, Rapid City, S. D.

Wilheit, T. T., M. S. V. Rao, T. C. Chang, E. B. Rodgers and J. S. Theon, 1975: A satellite technique for quantitatively mapping rainfall rates over the oceans, X-911-75-72, NASA Goddard Space Flight Center.